UCLouvain

epl

École polytechnique de Louvain

# Robust and adaptive reaching control in human:

## Modulation of control strategies across contexts

Author: **Héloïse Dehem**
Supervisor: **Frédéric Crevecoeur**
Readers: **Renaud Ronsse, Philippe Lefèvre**
Academic year 2019–2020
Master [120] in Mathematical Engineering

# Abstract

This master thesis investigates the modulation of the control strategy used by the central nervous system (CNS) during human reaching movements across contexts. An experiment was conducted to analyse the changes in robust and adaptive control across changes in environment uncertainty. Seven participants took part in the experiment and were asked to perform reaching movements, called trials, in two different contexts. During both parts of the experiment, participants were told that their hand movements would be perturbed during random trials. The two parts of the experiment differed in environment uncertainty, i.e. in the number and types of perturbations applied during random trials. We discovered that a more robust strategy is used in a less predictable context, at the expense of adaptation.

# Acknowledgements

First, I would like to thank my supervisor Professor F. Crevecoeur for his support and precious help throughout the year. It was a real opportunity to conduct an experience in the field of motor control while having the support needed.

I would also like to thank Professor P. Lefèvre and Professor R. Ronsse for agreeing to be part of my thesis jury.

Last but not least, I would like to thank all of the experimental subjects who took part in my experience: Charlotte Assenmacher, Laurent Blondeau, Victoria Bosly, Guillaume Claes, Isabel Herbert, Enat Wauthy and Ysaline Willard.

# Contents

# List of abbreviations

**CNS** Central nervous system

**LQG** Linear Quadratic Control

**FF** Force field

**CW** Clockwise

**CCW** Counter-clockwise

**PM** Pectoralis major

**PD** Posterior deltoid

**EMG** Electromyography

**DF** Degrees of freedom

**SD** Standard deviation

# List of Figures

# List of Tables

# Chapter 1

# Introduction

Reaching movements are the basis of our everyday lives. When washing the dishes, doing the groceries, writing an essay, or picking up a fallen pen, complex interactions occur between our brain and muscles to ensure the smooth running of the task. Our brain, and more precisely central nervous system (CNS), has to compute a command signal for our muscles not only based on the movement dynamics of our body and its surroundings, but also based on possible perturbations that may occur.

In the 2019 paper "Robust Control in Human Reaching Movements: A Model- Free Strategy to Compensate for Unpredictable Disturbances" [8], it was suggested that when executing reaching movements, participants modify their control strategy depending on the context. Two different reaching experiments were conducted showing different control strategies for different contexts. In a less predictable context, obtained by increasing the frequency and number of different types of perturbations applied during reaching movements, more vigorous responses were noticed. The increase in movement vigour, was measurable by the increase in movement velocities and feedback responses. This change of strategy was linked to a robust control that reduces the sensitivity to disturbances. Simultaneously, a second change of strategy was noticed when switching to a less predictable context. Adaptation, which represents the CNS's ability to anticipate a perturbation based on preceding reaching movements, decreased when the context became less predictable.

These results suggest that, to some extent, a trade-off exists between robust control and adaptation, such that a more robust strategy can be selected by the CNS at the expense of one's faculty to adapt. However, because the participants tested were not the same in both contexts, it is impossible to determine whether these strategy changes were indeed due to the change of context or simply due to the change of participants. Therefore, the question on how the CNS modulates its control strategy based on the context remains, and it is the objective of this master thesis to answer it. More specifically, the goal of this thesis is to analyse how robust and adaptive control evolve in human reaching tasks across different contexts. To find out, the same experiment as in the 2019 paper [8] was conducted but testing the same participants in both contexts. The work of this thesis is therefore strongly linked to the 2019 paper on robust control in reaching movements, and throughout this work it will often be referred to.

In this section, we will begin by presenting an illustrative example, to clarify the question we are trying to answer. Next, our motivations will be presented. Thereafter, we will

briefly discuss the experiment that will be conducted to answer this question. We will finish off with an outline of what will be presented throughout this master thesis.

## 1.1 Illustrative example

Consider a professional wrestler. When in the fighting ring, the goal of a wrestler is to beat his opponent. To do so, he will have to try and bring his opponent to the ground by grabbing him. However, while trying to do so, the opponent will defend himself and deflect the attacker's approach. The wrestler has to try and achieve a reaching task while in a very unpredictable environment. It is our hypothesis, based on the 2019 paper, that this will lead to a very different control strategy than the one used in a more predictable environment. Indeed, if the same wrestler were to do his groceries, he would not grab his articles out of the aisles in the same manner he would try and grab his opponent on the wrestling ring.

The aim of this thesis is to understand just how an individual modulates his control strategy depending on the context.

## 1.2 Motivation

The work of this thesis is enclosed in the large and complicated field of motor control. The study of motor control consists in exploring how the central nervous system interacts both with the environment and the muscles it wishes to control to produce the desired movements [19]. The current motor control models are used to further understand different neurological movement disorders and develop appropriate treatment strategies. Motor control theory also plays an important role in choosing the best rehabilitation protocol for motor-impaired patients, such as stroke patients [6].

More specifically, the study of the modulation of the control strategy across contexts can help determine the best conditions for rehabilitation, i.e. the interventions that will maximise the rate of motor learning and help patients achieve the best functional recovery possible [6].

## 1.3 Experiment

The experiment that was conducted in the framework of this master thesis is based on the experiment described in the 2019 paper on robust control in reaching movements [8]. The experiment of the 2019 paper was divided into two parts, called experiment 1 and experiment 2. During both parts, participants performed series of 60 hand reaching movements, called trials, holding the handle of a KINARM robot. Participants were told that during random trials they would be perturbed by the robot during their reaching movements, but were not told how or how often. Experiment 1 and experiment 2 differed in the number of trials that were perturbed per series of 60 trials. They also differed in the number of different types of perturbations applied to the hand during reaching movements. This created a difference in environment predictability between both phases of the experiment, allowing the analysis of the modulation of the control strategy across

both contexts.

In the 2019 paper on robust control, it was observed that the control strategy used and the rate of adaptation differed across context. In a more predictable environment, in which less reaching movements were affected by perturbations, participants seemed to use a less robust strategy, as their hand paths were more deviated by unpredictable disturbances. Simultaneously, it was observed that each perturbation had a larger impact on the following trial, meaning that a larger rate of adaptation was used. Participants anticipated a larger fraction of the force field that they just experienced in a more predictable environment. The impact of a perturbation on the following trial is called after-effect and it is the signature of motor adaptation. When a second group of participants executed the same reaching movements in a less predictable environment, they were noticed to use a more robust strategy but displayed smaller after-effects. Therefore, there seemed to be a negative correlation between robustness and adaptation across experiments, as a more robust strategy seemed to be paired with less adaptation. The question was raised whether this reflects a trade-off in neural circuits.

However, the study conducted in the 2019 paper could not answer this question, because two different groups of subjects participated in the two experiments. Therefore, it was impossible to determine whether the changes in strategy and learning had indeed occurred due to the change of context or if they were simply due to the change of subjects. To address this problem, the same experiment was conducted in the framework of this master thesis but with the same group of subjects taking part in both experiments. This allowed us to determine whether the results obtained were indeed due to the change of context or if they were simply due to the change of subjects.

## 1.4 Outline

We will start this thesis by presenting the state of the art on human reaching movements in chapter 2. The basic concepts that are needed to understand this work will be thoroughly presented. Next, we will describe the experiment that was conducted in chapter 3. Chapter 4 will summarize the results obtained during this experiment. These results will then be discussed in chapter 5, along with some further perspectives on work that can be done to improve our results. Finally, chapter 6 will expose the main conclusions of this thesis.

# Chapter 2

# State of the art

We begin this work by studying the state of the art on human reaching movements and their response to unpredictable disturbances. To begin, a general summary on optimal feedback control will be presented, as it is an influential model and it will play an important role in the interpretation of our results. Furthermore, we will discuss the impact of unmodelled disturbances on the control strategy, and more precisely the concepts of adaptation and robust control. Finally, we will finish off by discussing how all these concepts fit together in the context of reaching tasks.

## 2.1 Optimal feedback control

Motor behaviour, such as a simple movement of the arm, is the result of complex interactions between limb mechanics and neural control, which takes place in the central nervous system (CNS) [23]. The interactions between these three aspects - motor behaviour, limb mechanics and neural control - can be described by optimal feedback control theory. The goal of optimal control is to find the control signals that will impact a dynamical system in a way that optimizes a certain performance criterion while satisfying the dynamical constraints of the system [14]. The control signals are computed using the feedback that is sent from the system to the controller. In the context of human reaching movements, the CNS acts as the controller and the arm is the system that is steered to achieve the desired task. Figure 2.1 illustrates the interactions between the CNS and the system in optimal feedback control.

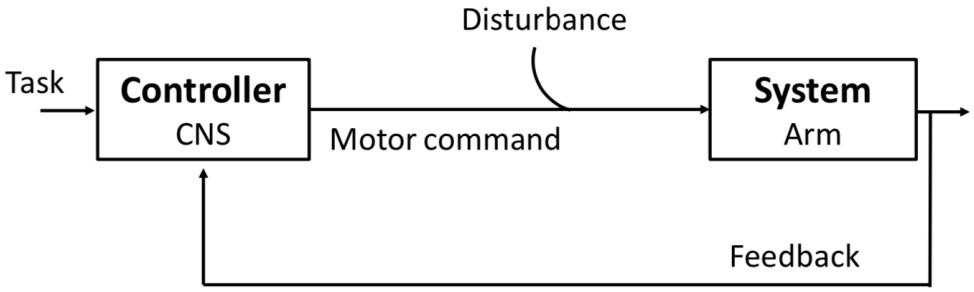


**Figure 2.1:** Optimal feedback control: Schematic representation of optimal feedback control as model of neural control of human reaching movements. The controller is the CNS and the system is the arm.

To achieve the desired task, the controller uses an internal representation of the movement

dynamics of the system, in this case the arm, to compute the command control. In this section, we will first present a linear model of the arm that was introduced in the 2019 paper on robust control. We will then discuss the different control models that can be used to model the control strategy used by the CNS.

### 2.1.1 Linear model of the arm

To fully understand the work of the controller, it is important to understand how the controller perceives the system. In the framework of the 2019 paper on robust control, a linear state-space representation of the arm was considered, as it is imposed by the limitations of current control theories [8]. The linear model described in this section was used in the 2019 paper on robust control to validate the concepts that are further developed in this paper. It is important to describe this linear model to fully understand the concepts described throughout this work.

The movement of the arm was modelled by the translation of a 1 kg point mass in a horizontal plane against dissipative viscous forces. The model used considered that a force field could be applied to the system as a perturbation. The controlled force, which represents the force applied by the arm muscles, was modelled based on the control command using a linear approximation of the muscle dynamics. The continuous-time differential equations of the model were as follows:

$$\ddot{x} = -k\dot{x} + \theta_x\dot{y} + F_x \tag{2.1}$$

$$\ddot{y} = -k\dot{y} + \theta_y\dot{x} + F_y \tag{2.2}$$

$$\tau\dot{F}_x = u_x - F_x \tag{2.3}$$

$$\tau\dot{F}_y = u_y - F_y \tag{2.4}$$

where x and y represent the coordinates of the horizontal plane in which the translation movements occur. The variables $u_x$ and $u_y$ represent the control commands sent by the CNS and $F_x$ and $F_y$ the corresponding controlled forces exerted by the muscles. The parameters $\tau$ and $k$ represent the time constant of the linear muscle model and the viscous constant. $\theta_x$ and $\theta_y$ are parameters used to define the force field applied to the point mass during the translation movement. When no force field is applied, they are both equal to 0. If however a certain force field is applied, they differ from zero and describe the applied force field. In the framework of reaching movements affected by unmodelled disturbances, the controller has no information on the values of $\theta_x$ and $\theta_y$. These unknown parameters are what cause the system dynamics to be unpredictable. The state-space representation (equations 2.1 - 2.4) can be rewritten in way that highlights the uncertainty of the dynamics linked to perturbations:

$$\dot{\mathbf{x}} = (A + \Delta A)\mathbf{x} + B\mathbf{u} \tag{2.5}$$

where the state vector is defined as $\mathbf{x} = [x, y, \dot{x}, \dot{y}, F_x, F_y]^T$ and the control vector as $\mathbf{u} = [u_x, u_y]^T$. In equation 2.5, $A$ represents the model dynamics when no force field is applied, and $\Delta A$ the model disturbance which occurs due to an unknown force field ($\theta_x$, $\theta_y$). The model disturbance $\Delta A$ is unknown to the controller.

Besides unmodelled perturbations, the system dynamics can also be impacted by noise. Taking noise into account, we can rewrite equation 2.5 based on instantaneous differences instead of time derivatives:

$$d\mathbf{x} = [(A + \Delta A)\mathbf{x} + B\mathbf{u}]dt + Cd\mathbf{w} \tag{2.6}$$

where $Cd\mathbf{w}$ represents the stochastic disturbances applied to the system due to noise. We can define $\epsilon(\mathbf{x}, \mathbf{w}) \coloneqq \Delta A\mathbf{x} + Cd\mathbf{w}$, the total unknown disturbance of the system, and rearrange the terms to isolate $\epsilon$. This unknown disturbance takes into account both the model perturbation ($\Delta A$), which is a fixed model error, and the noise-related perturbation ($Cd\mathbf{w}$), which follows a zero-mean Gaussian distribution. To highlight the model uncertainties, equation 2.6 can be written as the sum of the known model dynamics and the unknown disturbance function :

$$d\mathbf{x} = [A\mathbf{x} + B\mathbf{u}]dt + \epsilon(\mathbf{x}, \mathbf{w}) \tag{2.7}$$

Equation 2.7 illustrates the problem of control with unknown model errors in line with our experiment. When controlling the arm, the CNS uses it's internal representation of the movement dynamics to compute the command control $\mathbf{u}$. Equation 2.7 allows us to model the CNS's knowledge on the limb dynamics (A and B) and the error term which is unknown to the controller ($\epsilon(\mathbf{x}, \mathbf{w})$). We assume that a neural representation with a similar structure is used by the brain.

### 2.1.2 CNS as controller

The CNS acts as our body's controller. It computes a command based on the given task and the feedback received from the system, in this case our arm, which steers the system in the desired direction. Different models of optimal control exist, each considering a different cost function to be optimized. Based on this cost function, a time-varying control law is computed.

LQG, linear quadratic Gaussian control, is a model of neural feedback control that is frequently used. It minimizes the cost of movements while considering that the system is affected by noise that follows a zero-mean Gaussian distribution. In other words, LQG control is based on the hypothesis that the unknown disturbance function $\epsilon(\mathbf{x}, \mathbf{w})$ as defined in equation 2.7 does not contain a fixed model error ($\Delta A = 0$). It is assumed that the unknown disturbance function only includes the noise related perturbation $Cd\mathbf{w}$, and therefore follows a Gaussian distribution. When an unmodelled perturbation is applied to the system, a fixed model error is added to the unknown disturbance function. Because the unknown disturbance function does not have a Gaussian distribution anymore, the LQG assumptions are violated. LQG control is not the best solution to the optimal feedback control problem anymore. In the framework of reaching movements affected by unmodelled perturbations, it is thus more suitable to consider a control strategy that is less sensitive to fixed model errors, such as robust control.

Robust control is a model-free design. It is said to be "model-free" because no knowledge on the disturbance function $\epsilon(\mathbf{x}, \mathbf{w})$ is needed. Different designs of robust control exist; in the framework of the 2019 paper on robust control, it was chosen to work with a robust control design based on game-theoretic principles ($\mathcal{H}_\infty$ [3]).

In the $\mathcal{H}_\infty$ design of robust control, the worst-case cost function, i.e. the cost function associated to the worst-case disturbance, is minimized [8]. To do so, the robust controller considers that a fictive player is trying to maximize that same cost function by modulating the disturbances applied to the system. The robust controller then computes a command signal which minimizes this maximum. Thus, the robust controller acts as a mini-max feedback controller as it minimizes the cost function assuming worst-case uncertainty [27].

This robust control design is convenient, as it is an extension of the LQG control, allowing us to consider the same system and cost function. Only the assumptions on the error term $\epsilon$ are changed. However, a disadvantage of this control design is that it forces us to work with a linear state-space representation, as described in section 2.1.1.

It is important to note that both controllers (LQG and robust controller) are solutions of the optimal feedback control problem, each useful in different contexts. Indeed, LQG leads to efficient movements when considering Gaussian noise disturbances but doesn't respond well to arbitrary disturbances, i.e. disturbances that are not gaussian distributed and that cause a fixed model error. On the other hand, the robust controller generates movements that are less sensitive to arbitrary disturbances but that are costlier [8]. This is a well-known tradeoff between efficiency and sensitivity to model errors, which occur due to perturbations, in optimal control.

## 2.2 Human reaching control strategies

When performing reaching movements, the CNS uses its internal representation of the movement dynamics, defined by $A$ in equation 2.7, to achieve its tasks. When confronted with an unpredictable change in movement dynamics, the dynamics are altered by an unknown fixed model error $\Delta A$. A gap is created between the actual movement dynamics $(A + \Delta A)$ and the CNS's internal representation $(A)$, resulting in strongly deviated hand paths. This gap, created by the unexpected dynamics, is handled differently according to the control strategy that is used by the CNS.

It is important to understand how these changes in movement dynamics $\Delta A$ can occur. First, gradual variations of the arm dynamics occur during development, as the bones grow and the muscle mass increases [24]. Moreover, the arm dynamics can vary in a shorter time scale, as a result of fatigue for instance. External perturbations, such as force fields applied to the arm, also result in changes in the movement dynamics. For instance, when grabbing a tool for the first time, the torque loads corresponding to the mass distribution of this new tool are unknown to the controller. All of these changes in movement dynamics result in different motor behaviours for the same applied muscle forces. Therefore, the controller needs to handle these unexpected changes to maintain the desired performance.

As explained in the introduction, the goal of this thesis is to analyse the modulation of the control strategy used by the CNS across contexts. More precisely, we wish to analyse how the CNS handles unexpected dynamics, as defined by $\Delta A$ in equation 2.7, depending on the context.

Before looking into the context's influence on reaching movements, it is necessary to understand what the different control strategies are. In this section we will present two

control strategies discussed in the 2019 paper: *adaptive control* and *robust control*. Both deal with the unexpected dynamics in their own way. It is important to note that both of these strategies can happen simultaneously. However, in section 5 we will notice that adaptation seems to be reduced when a more robust strategy is selected.

### 2.2.1 Adaptive control

A first strategy used by the CNS to deal with these unexpected dynamics, is called adaptation. It consists in trying to learn the fixed model error $\Delta A$. The CNS' ability to adapt its internal representation of the movement dynamics following a disturbance is called motor learning or error-based adaptation. It is the capacity to anticipate the movement dynamics of a reaching movement, based on the previous reaching tasks. A schematic representation of adaptation is presented in figure 2.2.

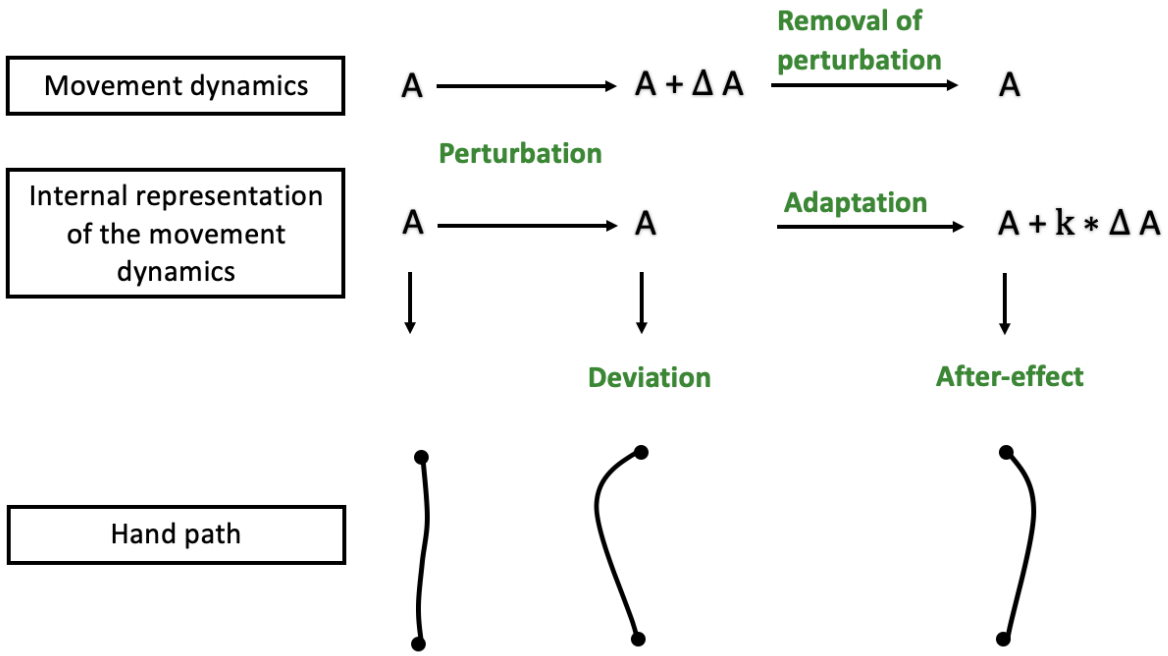


**Figure 2.2:** Adaptation: Schematic representation of adaptation to novel movement dynamics due to a perturbation. Illustration of the hand deviation before, during and after a perturbation is applied. The after-effect occurs in the opposite direction than the original deviation due to the perturbation.

If a perturbation is applied during a reaching movement, the change in movement dynamics $(A + \Delta A)$ will cause a deviation in the hand path, due to the gap between these new movement dynamics and the CNS' internal representation $(A)$. Following the perturbation, the CNS will learn, at least partially, the new movement dynamics $(A + \Delta A)$ by updating its internal representation :

$$A' = A + k * \Delta A \tag{2.8}$$

with $k$ indicating to which extent the new dynamics are learnt. The controller adapts its internal representation of the movement dynamics according to the experienced disturbance, in a way that would allow it to counter that same disturbance.

If the perturbation is then removed, setting the actual movement dynamics back to $A$, a new gap occurs between the actual dynamics ($A$) and the internal representation of the CNS ($A + k * \Delta A$). The new gap ($-k\Delta A$) and the old gap ($\Delta A$) are thus of opposite sign. Therefore, a lateral deviation in the opposite direction than the perturbation occurs after the sudden removal of that perturbation [24]. This lateral deviation is called after-effect, and it is the tool that is used to measure adaptation. Adaptation to a certain perturbation can thus be measured by the after-effect that occurs during the next reaching movement.

The variable k indicates to which extent the new dynamics are learnt. Bigger k-values will lead to bigger after-effects. Furthermore, repeated exposure to a same perturbation leads to repeated adaptation to that same perturbation, which further reduces the gap between the actual movement dynamics and the internal representation of the CNS. Thus, repeated exposure to a same perturbation also leads to larger after-effects. Therefore, trial-by-trial changes in after-effect suggest a change in rate of adaptation k, or a build up due to successive adaptations. The variable k and its values will be further discussed in chapter 5.

### 2.2.2 Robust control

A second strategy used by the CNS to handle unexpected dynamics $\Delta A$, is robust control. As explained in section 2.1.2, robust control is a form of optimal feedback control where the cost function is minimized assuming a worst-case perturbation. No model of the perturbation function as defined in equation 2.7 is needed, and so no knowledge on $\Delta A$ is needed either. Therefore, as opposed to adaptation, robust control is insensitive to fixed model errors.

In the framework of optimal control, the motor command is computed based on the sensory feedback that is received from the system, as shown in figure 2.1, and a state estimator. Therefore the motor command, also called the feedback control signal, is affected by experienced perturbations, with as factor the control gains. For a given perturbation, higher control gains will lead to a higher command signal. Thus, control gains determine the impact that the perturbation will have on the command, and by modifying the control gains, we modify how the controller reacts to perturbations. Higher control gains lead to a controller that is less sensitive to disturbances. Therefore, when dealing with unpredictable model errors $\Delta A$, increasing the control gains makes the controller more robust to perturbations.

In the framework of the experiment presented in the 2019 paper on robust control [8], these changes in control gains were measured by a change in speed and robustness to perturbations during trials. It was noticed that an increase in control gains leads to an increase in speed and a more vigorous response. Robust control predicts an increase in control gains following a perturbation, making the controller less sensitive to disturbances. Just like adaptive control, robust control leads to trial-by-trial changes in limb motion, measured by changes in speed and robustness to perturbations.

An important question is how are these behaviours implemented in the neural circuits. A possible answer was found by analysing muscle activities, as it was noticed that co-contraction, which refers to the simultaneous activation of muscles with opposite actions,

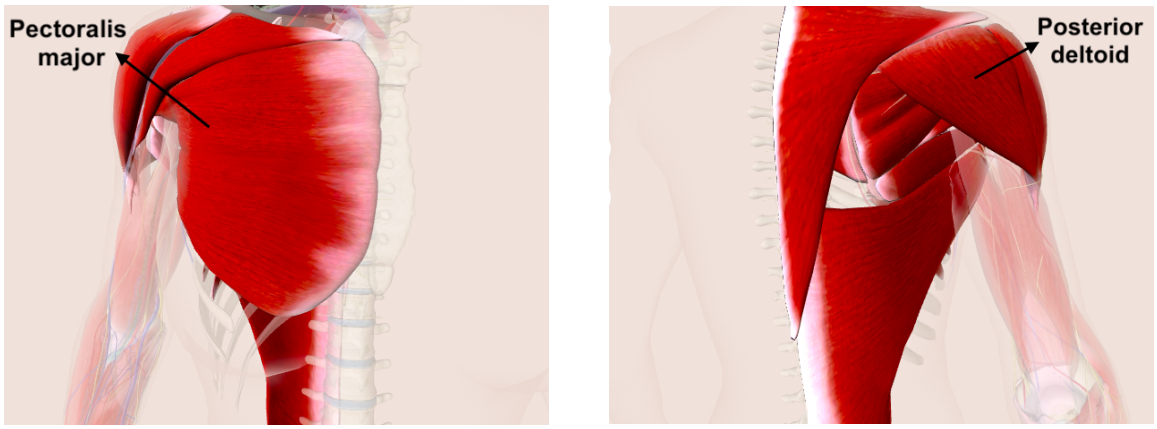


**(a)** Front view - Pectoralis major **(b)** Back view - Posterior deltoid

**Figure 2.3:** Pectoralis major and posterior deltoid muscles [18].

was correlated with the increase in forward velocity [8].

### Co-contraction

Co-contraction is the simultaneous contraction of two or more muscles around a joint. In the context of reaching movements, the two muscles are the pectoralis major and posterior deltoid, illustrated in figure 2.3. The co-contraction of muscles is measurable by their simultaneous increase of activity. The minimum activity across muscles is used as an indication of the level of co-contraction [8].

Originally, it was assumed that co-contraction is used to alter the intrinsic properties of the muscles to make the joints rigid [5][12]. This strategy, called impedance control or predictive control, assumes that stability is achieved by controlling the mechanical impedance of the limb through co-contraction. The mechanical impedance of the limb refers to the muscles intrinsic visco-elastic properties. These intrinsic visco-elastic properties can be illustrated as the combination of the properties of a spring (elastic) and a dashpot (viscous) [11]. When affected by a load, a spring instantaneously produces a deformation proportional to the load [13]. A dashpot, produces a velocity proportional to the load at any instant. The visco-elastic properties of a muscle, thus refer to its ability to oppose to changes in velocity and position. The impedance control design which was originally suggested to explain co-contraction, assumes that the visco-elastic properties of the muscle are altered through co-contraction to achieve stability. More specifically, it was suggested that the magnitude, shape and orientation of the endpoint stiffness of the arm can be controlled by co-contraction to encounter unpredictable disturbances. The endpoint stiffness of the arm is a mechanical property that characterizes the arm's resistance to disturbances encountered in the environment [4].

This theory was validated in a paper published in 2001 [5]. In this paper, the question on how the CNS could stabilize the hand movements in unstable dynamics was raised. More specifically, it was noted that neural feedback is delayed by the sensory feedback pathways and that therefore, feedback control couldn't be responsible for instantaneous stabilisation of hand movements. It is in this context that impedance control was suggested. Later, in a paper published in 2003, this theory was further developed [12]. It was suggested that

impedance control occurred in parallel with a second separate motor control mechanism: the inverse dynamics model. The paper states that when faced with unexpected dynamics, the controller first increases the muscle impedance to stabilize the arm during the earliest phase of learning. Then, once the inverse dynamics model has been acquired, the muscle impedance is decreased.

Both of these papers suggested that impedance control has an important role in the stabilisation of hand movements. However, this hypothesis was later criticized. Indeed, the contribution of intrinsic impedance during feedback responses to disturbances was questioned [7]. In the 2001 article on impedance control, the impedance was measured by analysing the motor responses to perturbations, which includes the motor responses that occur due to neural feedback. Thus, the impact of the muscles intrinsic properties was overestimated. This was in fact already stated in a paper published in 2000 in which the muscle stiffness was computed. In this paper, it was mentioned that the stiffness of the muscles depends on the reflexes, and thus on the feedback loop [4]. In a paper published in 2014, it was therefore suggested that the intrinsic properties of muscles only slightly contribute to force feedback in comparison with neural feedback, indicating that impedance control does not handle unexpected dynamics as well as originally predicted [7]. The utility of co-contraction was thus re-evaluated. In this paper, it was suggested that co-contraction is rather used to impact the reflex gains.

Indeed, the increase in baseline muscle activity leads to an increase in reflex gains [20]. The process of increasing the control gains by increasing the baseline muscle activity is called "gain-scaling". It is the fact that a difference in baseline muscle activity levels leads to a difference in response to a same perturbation.

In the 2019 paper on robust control in reaching movements, it was suggested that gain-scaling is used to implement the changes in control gains that were noticed, as these changes correlated with co-contraction [8]. Indeed, an increase in activity of both muscles was measured following a perturbation trial, which correlated with the increase in forward velocities. Therefore, it was suggested that co-contraction is the process used by the CNS to increase the control gains.

A second advantage of co-contraction was noticed, which is that the increase in muscle activity also increases the range of the feedback responses. To understand how, one must first understand the interactions between two muscles working at the same joint. In the context of human reaching movements, it is the posterior deltoid and pectoralis major muscles that are of use, both part of the shoulder joint as illustrated in figure 2.3. When performing a movement in a certain direction, the muscle performing the action is called agonist. The second muscle, which has the capacity to oppose the movement of the first (agonist) muscle, is called the antagonist muscle. Both muscles can be agonist or antagonist, depending on the movement performed by the arm. If the baseline activity of both muscles is at its lowest, both muscles can only perform a movement in a certain direction. More specifically, the antagonist muscle can only counter the agonist muscle during a movement. However, if the baseline activity of both muscles is increased, the antagonist muscle can accompany the agonist muscle in its movement. An increase in baseline muscle activity enables both stretch- and shortening responses in antagonist muscles, allowing it to help the agonist muscle achieve the desired movement [8]. There-

fore, the elevation of levels of muscle activity lead to an increase in feedback response range.

To summarize, it was suggested in the 2019 paper on robust control that co-contraction has two different consequences on reaching movements, both increasing the control gains . First, co-contraction enables gain-scaling, which leads to larger reflex responses. Additionally, co-contraction enables a decrease in activity of the antagonist muscle, which increases the feedback response range.

# Chapter 3

# Materials and methods

The purpose of the experiment was to analyse the changes in control strategies across contexts.

## 3.1 Experimental setup

Seven healthy right-handed subjects, ranging in age from 21 to 55 years (2 males, 5 females), participated in this study. Participants were seated in front of a KINARM robot and were asked to grab the handle of the robot with their right hand, as shown in figure 3.1.


**Figure 3.1:** KINARM robot [16].

The KINARM robot possesses a video display monitor mounted above the robot's handle, allowing the subjects to see their hand movements by virtue of a hand-aligned cursor displayed on the screen. The screen was also used to indicate the starting position and targets for the reaching movements. The KINARM workspace is represented in figure 3.2.

## 3.2 Experimental procedure

The experiment consisted of two phases: the low frequency experiment and the high frequency experiment. All participants went through both phases. Four subjects first

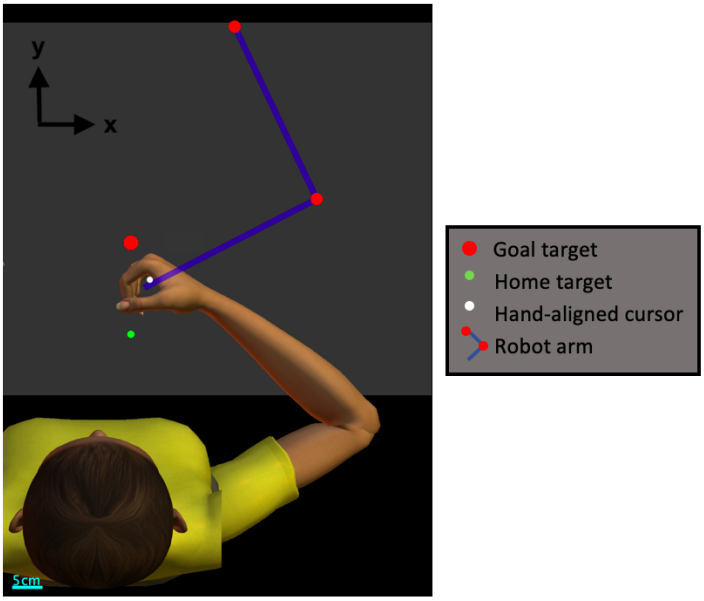


**Figure 3.2:** KINARM workspace.

completed the low frequency experiment and then proceeded to the high frequency experiment, and 3 subjects went through both phases in the opposite order. This was to make sure the order of the phases wouldn't impact our results. All participants also completed a calibration block in between both experiments, which was later used to normalize the muscle activities measured.

In both experiments, the task instructions were the same. Participants had to grab the handle of the robot with their right hand and carry out reaching movements based on the hand-aligned cursor that was visible on the KINARM display. The reaching movements consisted in 15 cm forward reaches between the home target and the goal target, that were positioned as represented in figure 3.2.

The home target was closest to the participant, and was represented by a circle of radius 0.6 cm, which was originally red. The goal target was located 15 cm further away from the participant than the home target, and was represented by a circle of radius 1.2 cm, which was originally an open red circle.

Participants were instructed to first move the cursor into the home target, which once it was attained turned green. Then, participants were to wait for the go signal, which would appear after a random delay following their stabilization into the home target of 2 to 4 seconds and which was uniformly distributed. The go signal was implemented by having the open red circle of the goal target turn into a filled red circle. This go signal informed the participants that they should start their reaching movement towards the goal target. The aim was for the participants to reach the target in a time lapse of 0.6 to 0.8 seconds after the go-signal was given. Once the goal target was reached, participants had to stabilize the hand cursor in the target for 1 second for the reaching task to be successful.

Three different scenarios were possible. If the participant were to reach the goal target

too early, that is in less than 0.6 seconds, the target would turn back to an open red circle. If the participants reached the goal target in the prescribed time window, that is in 0.6 to 0.8 seconds, the goal target would turn green. Finally, if the participants reached the goal target too late, that is in more than 0.8 seconds, the goal target would remain red. This allowed participants to monitor their speed, making it possible to maintain similar movement speeds throughout the trials. However, all trials were kept and used in the analysis of the data. The step-by-step unfolding of a trial is illustrated in figure 3.3.

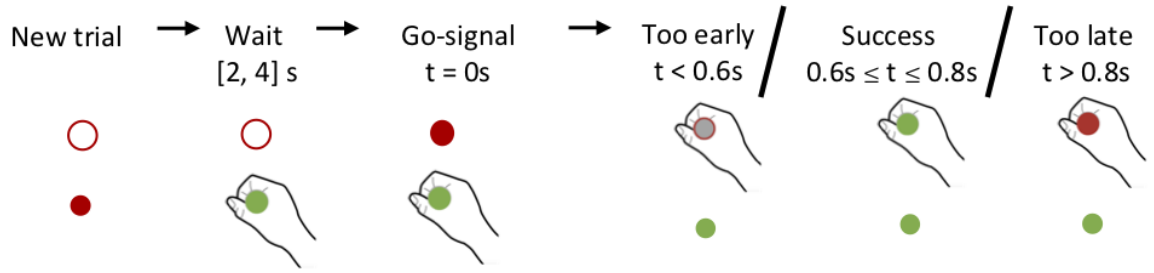


**Figure 3.3:** Trial procedure. Step-by-step unfolding of a trial. Adapted from [8].

During both experiments, high and low frequency, perturbations were applied on the robot handle at random trials. Therefore during both experiments, the movement dynamics were unpredictable and varied throughout the trials. Throughout this work, we call the trials performed in the null field, that is without any perturbations applied during the movement, baseline trials.

Before starting the experiments of both phases, participants were allowed to practise their reaching movements in the null field. They each performed a series of about 20 baseline trials to get comfortable with the reaching task. Once they felt ready, they completed both phases in one of the two orders, either starting with the low or high frequency experiment. Both phases consisted of a series of 4 blocks of 60 trials. Participants were told that during these 4 blocks, the KINARM robot could perturb their movements, but were not told how or how often.

### 3.2.1 Low frequency experiment

During the low frequency experiment, each block of trials was composed of 50 null field trials and 10 force field trials, which occurred in a random order. The force field trials were trials were a curl force field was applied to the robot handle during the movement. The curl force field applied during force field trials generated perturbation forces relative to the movement velocities in the following way:

$$\begin{bmatrix} F_x \\ F_y \end{bmatrix} = \begin{bmatrix} 0 & L \\ -L & 0 \end{bmatrix} \begin{bmatrix} \dot{x} \\ \dot{y} \end{bmatrix} \tag{3.1}$$

where the $x$ and $y$ axes are defined according to figure 3.2. $F_x$ and $F_y$ represent the $x$ and $y$ component of the perturbation force, $\dot{x}$ and $\dot{y}$ represent the movement velocities in both directions, and L represents the curl force field factor. Five of the ten force field trials were clockwise (CW) and the other five were counterclockwise (CCW). For CW trials L

was equal to 15 Ns/m and for CCW trials it was equal to -15 Ns/m. The impact of a curl force field, CW or CCW, on the hand path is illustrated in figure 3.4.

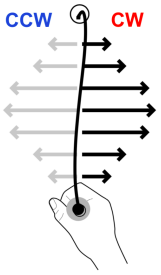


**Figure 3.4:** Curl force field trial. Adapted from [8].

### 3.2.2 High frequency experiment

The goal of the high frequency experiment was to increase the uncertainty of the movement dynamics compared to the low frequency experiment. This was done both by increasing the number of perturbation trials and by having a wider range of types of perturbations. Each block was composed of 30 null field trials and 30 perturbed trials. Three different types of perturbations occurred: curl field perturbations, step load perturbations and orthogonal field perturbations. The curl field perturbations were the same as in the low frequency experiment; the perturbation force was computed according to equation 3.1. The step load perturbations were applied during null field trials when the participant's hand crossed a virtual line positioned at one-third of the distance between the home target and the goal target. This imaginary horizontal threshold line will be referred to as the threshold position throughout this work. The step perturbation consisted of a leftward or rightward constant load of 12 N, with a 10 ms linear buildup. The orthogonal field perturbations were applied using the following forces:

$$\begin{bmatrix} F_x \\ F_y \end{bmatrix} = \begin{bmatrix} 0 & L \\ 0 & 0 \end{bmatrix} \begin{bmatrix} \dot{x} \\ \dot{y} \end{bmatrix} \tag{3.2}$$

where the $x$ and $y$ axes are defined according to figure 3.2. $F_x$ and $F_y$ represent the $x$ and $y$ component of the perturbation force, $\dot{x}$ and $\dot{y}$ represent the movement velocities in both directions, and L represents the orthogonal force field factor. The orthogonal force fields were applied in both directions, with the orthogonal force field factor L worth either 13 Ns/m or -13 Ns/m. The impact of the orthogonal force field on the hand path is similar to the impact of the curl force field, without the y component of the force field. The impact of all three perturbations on the hand path is represented in figure 3.5.

Out of the 30 perturbed trials, 10 were curl field trials (5 CW and 5 CCW), 10 were step load trials (5 in each direction) and 10 were orthogonal field trials (5 in each direction). Just like in the low frequency experiment, the order of the 60 trials per block was completely random.

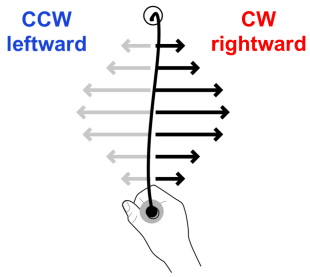


**(a)** Curl and orthogonal force field trials.

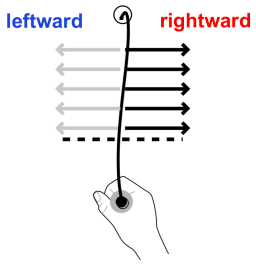


**(b)** Step load trials.

**Figure 3.5:** Curl, orthogonal and step load force field trials. Adapted from [8].

## 3.3 Data collection and treatment

The experiment was conducted using the KINARM End-Point Lab (BKIN Technologies), which is a facility used to study sensory, motor and cognitive function. Different measurements were collected and treated by the KINARM robot, in a similar manner than in the 2019 paper on robust control [8]. Both the components of the endpoint force and the coordinates of the hand-aligned cursor were collected and sampled at 1 kHz. The cursor velocity, which is equal to the hand velocity, was computed numerically using a fourth-order central-differences algorithm.

In both experiments, the muscle activity of both the pectoralis major and posterior deltoid was recorded, using electromyography (EMG). This was done by placing electrodes on both muscles, which were attached to the skin after light abrasion with alcohol. The signals measured were amplified by a gain of 1 k. They were then filtered using a sixth-order Butterworth filter (digital dual-pass filter; 15-400 Hz bandpass). Finally, the EMG signals were normalized using the calibration block which the participants performed between both experiments. This calibration block consisted of 6 trials. During these trials participants were asked to maintain postural control at the home target against a background load of 12 N. This background load was applied in both directions. It was applied in each direction during three out of the six trials. The average activity across 1 second recorded when participants maintained postural control at the home target was used to normalize the EMG signals.

The variables extracted were thus the hand kinematics, the forces applied to the robot handle and the EMG signals. These variables were averaged across trials and blocks for group data analysis.

## 3.4 Statistical analysis

To confirm our results, statistical tests were used. More specifically, the paired t-test and the repeated measures ANOVA test were used to determine whether a significant difference between the means of different groups exists, and the levene test was used to determine whether a significant difference between the variances of different groups exists. These tests were used throughout this master thesis to analyse changes in after-effect, forward velocity, robustness to perturbations and co-contraction both within a context and between contexts. All three statistical tests will briefly be discussed in this section.

### 3.4.1 Paired t-test

The paired t-test is a statistical test that compares the distributions of two observations of a dependent variable of the same subject [28]. Important assumptions are that the observations should be independent of each other and that the dependent variable should be approximately normally distributed. The goal of the t-test is to reject or confirm a null hypothesis, called $H_0$ which usually states that both measurements have the same mean. The alternative hypothesis $H_a$, can be directional or not, i.e. it can state that a difference exists between the means of both measurements with or without specifying the direction of this difference. When the alternative hypothesis is directional, the test is called a one-tailed paired t-test.

When computing a t-test, a p-value is computed. To obtain the p-value, a t-value is first calculated. The t-value is equal to the mean difference between the two observations of the dependent variable of each participant, divided by the standard deviation (SD) of these differences. Under the null hypothesis, this t-value should be an instance of the stochastic variable T which follows a t-distribution with n-1 degrees of freedom (DF), n being the number of participants. The p-value represents the probability of observing an instance of the stochastic variable T at least as extreme as the computed t-value, assuming T is a stochastic variable that follows a t-distribution with n-1 degrees of freedom.

Throughout this work the paired t-test was used to compare the after-effect, lateral deviation during force field trials, forward velocity and muscle activity of two different categories of trials. In all four cases a directional effect was predicted in theory and thus a one-tailed t-test was performed. The p-value was thus computed based on the t-value according to the predicted effect, i.e. $p = P(T > t)$ if $\mu_1 > \mu_2$ and $p = P(T < t)$ if $\mu_1 < \mu_2$.

The p-value computed indicates the probability of obtaining a variable distribution at least as extreme as the one measured assuming that the null hypothesis is true. Throughout this work we will use a threshold of 0.05 to validate of reject the null hypothesis. This means that if the computed p-value is inferior to 0.05, it will be assumed that it is (statistically) impossible that the null hypothesis is true, and thus the alternative hypothesis will be confirmed. If however the p-value is superior to 0.05, the null hypothesis will be maintained.

Because the sample size used in the experiment was quite small (n = 7), it is important to stay critical when analysing the results. Therefore, the effect size will also be measured, as it was suggested that small sample sizes should only be used if the effect size is large [10]. The effect size will be computed using Cohen's d value, i.e. it is the mean difference between the two groups divided by the standard deviation. It is considered large when it is larger than or equal to $\pm 0.8$.

### 3.4.2 Repeated measures ANOVA test

The ANOVA test is a statistical test that is very similar to the t-test, with as advantage that it can compare more than two groups of measurements. Just like when using a t-test, a p-value is computed to reject or confirm a certain null hypothesis $H_0$. This p-value is computed based on an F-value, which represents the equivalent of the t-value of a paired t-test, for a repeated measures ANOVA test. The F-value is equal to the variance of the group means divided by the mean of the within group variances. This F-value is

compared to the F-distribution corresponding to the null hypothesis to obtain the p-value. A threshold value of 0.05 will be used to reject of confirm the null hypothesis, based on the p-value computed. Because the measurements that will be compared throughout this work are measurements of the same subjects, a *repeated* measures ANOVA test will be computed [28], which is the equivalent of a *paired* t-test used to compare more than two groups.

For each ANOVA test, the sphericity was tested using Mauchly's test, as it is an important assumption made when performing an ANOVA test. When it was noticed that this assumption was violated, sphericity corrections were applied and new p-values were computed.

Throughout this work the ANOVA test will be used to analyse the differences in peak velocity and EMG signals between both contexts.

### 3.4.3 Levene test

The levene test is a statistical test used to test the homogeneity of variances, i.e. it tests whether the population variances are equal. It can be used to compare differences in relative variation between two or more samples [22]. In the framework of this master thesis, it will be used to compare differences in the relative variation of the peak forward hand velocity as a function of the baseline index across experiment. Comparing the relative variation enables us to compare the variation independent of differences in sample means.

To test the homogeneity of variances, which is the null hypothesis of the levene test, a p-value is computed. The levene test is equivalent to an ANOVA test on the absolute value of the differences between a measurement and the mean of the group to which this measurement belongs. Therefore, just like for an ANOVA test, the p-value is calculated based on an F-value. Once again we will use the threshold value of 0.05 to confirm or reject the null hypothesis. The alternative hypothesis tested states that the variances of both populations, which in this case will be represented by both experiments, are not equal.

# Chapter 4

# Results

Altogether, the results obtained showed a change in control strategy linked to the change of context. This change in control strategy impacted the forward velocities, robustness to perturbations, co-contraction and after-effects measured. These changes reflected a more robust controller in a less predictable context, partially at the expense of adaptation. The results coincide with the results of the experiment of the 2019 paper on robust control, confirming our predictions.

In this section we will thoroughly present the results obtained. We will discuss all four parameters that were analysed : the after-effect of a perturbation, the forward velocity during reaching movements, the robustness of responses to perturbations and the co-contraction of the pectoralis major and posterior deltoid. For all four parameters, both the trial-by-trial changes within a certain context and the changes across contexts will be analysed. The results presented in this section will be discussed and analysed in chapter 5.

## 4.1 After-effect

As explained in section 2.2.1, the after-effect of a perturbation is the lateral deviation that occurs after sudden removal of that perturbation. It is a parameter that allows us to evaluate the level of adaptation of the controller. The after-effect is measured during baseline trials that follow perturbed trials. In this section we will present the different results obtained when measuring the after-effect. We will start with the results obtained in the low frequency experiment, indicating how the after-effect evolves within a block of trials. We will then present the results obtained when comparing the after-effect in both the low and high frequency experiments.

To analyse the evolution of the after-effect across trials, baseline trials were given an index based on the number of succeeding curl field trials in a specific direction that immediately preceded the baseline trial. Five different categories of baseline trials were considered based on this index: baseline trials of index 0, CW and CCW baseline trials of index 1, and CW and CCW baseline trials of index 2. The 'CW' and 'CCW' abbreviations indicate in which direction the preceding perturbations were oriented, clockwise (CW) or counter-clockwise (CCW). An illustration of the labelling procedure is visible on figure 4.1. Throughout this section, the same color code and indexing as in figure 4.1 will be used.

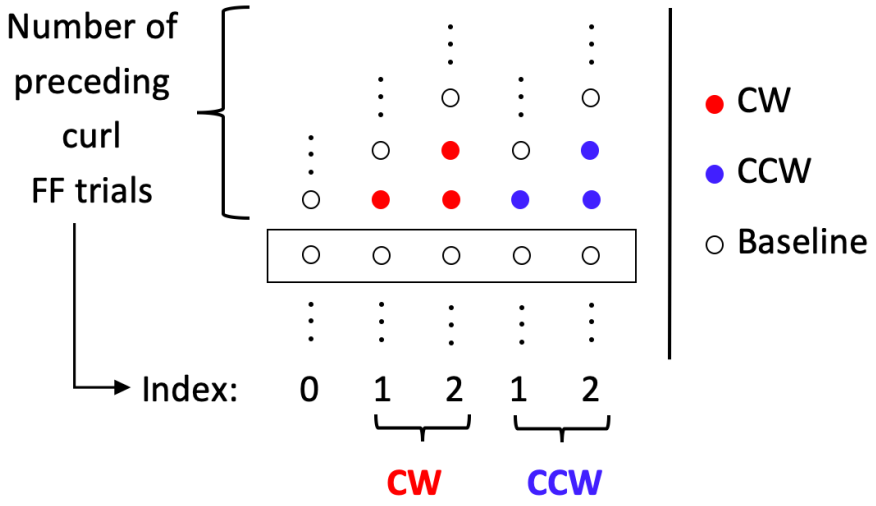


**Figure 4.1:** Labelling of baseline trials: Baseline trials were given an index based on the number of immediately preceding curl field trials of a same direction. Adapted from [8].

### 4.1.1 Trial-by-trial modulation

#### Low frequency experiment

The general phenomenon of adaptation can be illustrated by plotting the hand path of a trial affected by a perturbation and the following baseline trial, i.e. a trial during which no perturbation was applied. The after-effect is visible on the hand path of the baseline trial that follows the perturbed trial; it is the lateral deviation that occurs after removal of the perturbation. To illustrate this, all curl force field trials, separated into two categories according to the direction of the force field, were averaged across participants and plotted in figure 4.2. On the right of these force field plots, an average across all participants of all baseline trials that immediately followed these curl force field trials was plotted.

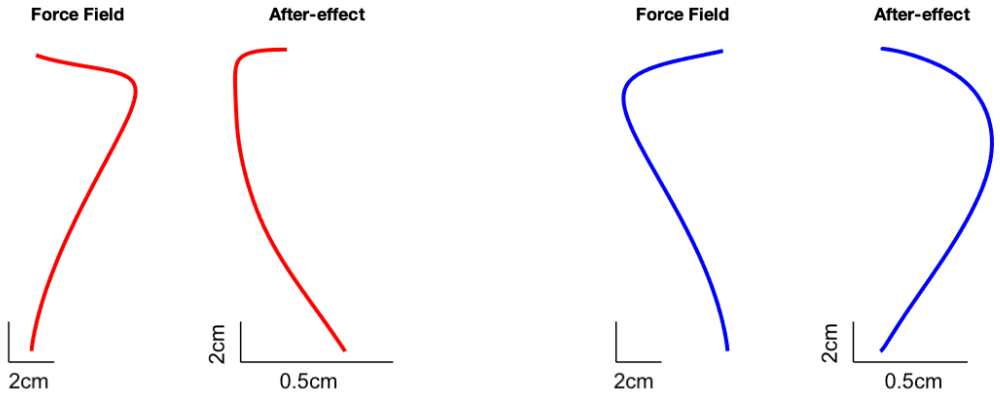


**(a)** Clockwise curl force field. **(b)** Counterclockwise curl force field.

**Figure 4.2:** After-effect. Data from the low frequency experiment. **(a)** Average across CW (red) curl FF trials (left-hand side) and immediately following baseline trials (right-hand side). **(b)** Average across CCW (blue) curl FF trials (left-hand side) and immediately following baseline trials (right-hand side).

Thus, figure 4.2 illustrates the after-effect that was noticed in trials following a curl force

field perturbation in the low frequency experiment. As predicted, the hand paths of baseline trials are deviated in the opposite direction than the immediately preceding perturbation.

A within context analysis of the evolution of the after-effect was performed for the low frequency experiment. More specifically, the after-effect due to curl force fields was measured both for trials of index 1 and trials of index 2. Figure 4.3 illustrates the average hand paths across all baseline trials of index 0, 1 and 2 both for preceding CW and CCW trials. The after-effect was evaluated as the lateral deviation at threshold position. The results obtained showed an increase in after-effect for an increase in baseline trial's index, as illustrated in figure 4.3.

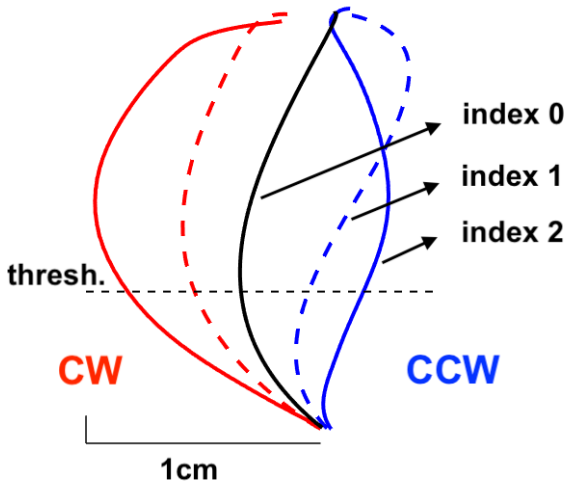


**Figure 4.3:** Trial-by-trial changes in after-effect. Illustration of hand path deviations of baseline trials following 0 (black), 1 (dashed) or 2 (solid), CW (red) or CCW (blue) curl FF trials. Data from the low frequency experiment.

To confirm these results, a paired t-test was performed between the lateral deviation at the threshold position of trials of index 0 and trials of index 1, for both clockwise and counter-clockwise perturbations. Trials of index 2 were not considered because there wasn't enough data, i.e. not all participants experienced CW and CCW baseline trials of index 2 in the low frequency experiment. The results of the paired t-test were the following:

| Paired t-test | p-value | effect size | t-value | DF | SD |
|---|---|---|---|---|---|
| *index 0 vs. index 1 [CCW]* | 0.0001 | 3.03 | 8.0170 | 6 | 0.0010 |
| *index 0 vs. index 1 [CW]* | 0.0023 | 1.66 | 4.3857 | 6 | 0.0013 |

**Table 4.1:** Trial-by-trial changes in after-effect. Results of paired t-test comparing the after-effect at threshold position of baseline trials of index 0 and 1, both for preceding CW and CCW curl force field trials. Data from the low frequency experiment.

Both p-values were significantly smaller than the threshold value of 0.05. It could thus be confirmed that trials of index 1 experienced a greater after-effect than trials of index 0, both for preceding clockwise and counter-clockwise curl force field trials. Furthermore, the

effect sizes measured were well above 0.8 indicating that the results were reliable.

Next, the level of adaptation was computed both for baseline trials of index 1 and baseline trials of index 2. This level of adaptation, represented by k in equation 2.8, indicates to which extent the internal model is updated. We decided to evaluate the level of adaptation by measuring the ratio of the after-effect due to a perturbation to the lateral deviation of that same perturbation. This was done by first computing the average lateral deviation at the threshold position of baseline trials which immediately followed one or two curl force field trials of a same kind. This value, which represents the after-effect of a baseline trial of index 1 or 2, was then divided by the average lateral deviation at the threshold position of the first curl force field trial to occur, i.e. the first of the two succeeding curl force field trials for baseline trials of index 2 and the first and only preceding curl force field trial for trials of index 1. Two levels of adaptations were computed, one for each baseline index (1 and 2). The computed levels of adaptation are gathered in table 4.2.

| | **Baseline trials of index 1** | **Baseline trials of index 2** |
|---|---|---|
| **Level of adaptation ∼k** | 0.2011 | 0.3992 |

**Table 4.2:** Trial-by-trial changes in level of adaptation to curl force field trials. Data from the low frequency experiment.

The results suggest that a baseline trial preceded by two succeeding perturbations is twice as adapted as a baseline trial preceded by a single perturbation.

### 4.1.2 Comparison across low and high frequency experiments

Next, a between-contexts analysis of the after-effect was performed. Both the changes in lateral deviation (after-effect) and the changes in level of adaptation (k) across contexts were analysed. The results obtained were also statistically proven.

#### Between context changes in after-effect

The average of the lateral deviation of the hand path at threshold position was computed for each index (0, 1 and 2), each direction (CW and CCW), each participant and for both contexts. The results obtained are plotted in figure 4.4. The black curves represent the mean lateral deviations across participants. Because the trials were performed in a random order, data for baseline trials of index 2 did not exist for all participants. A clear difference between both contexts was visible; the low frequency trials seemed to be more deviated.

To compare the after-effect in both experiments, a paired t-test was performed comparing the sum of the CW and CCW lateral deviations of all baseline trials of index larger than or equal to 1 at the threshold position. In other words, one value associated to the after-effect measured at the threshold position of trials that immediately succeeded a perturbation, was computed per subject in both contexts. These values were used to perform a one-tailed paired t-test between both contexts. The results obtained are gathered in table 4.3.

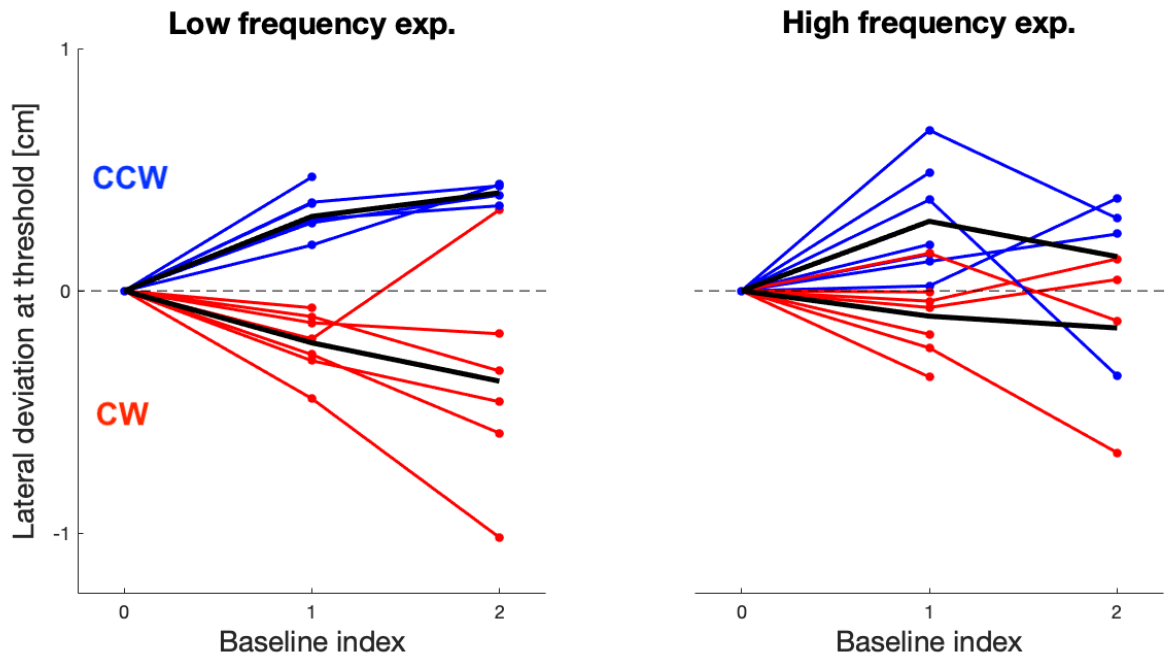


**Figure 4.4:** Context comparison: After-effect at threshold position. Lateral deviation at threshold position for each baseline index (0,1 or 2), direction (CW or CCW) and experiment, averaged across trials. Individuals' average across baseline trials of index 0 was subtracted in each experiment.

| Paired t-test | p-value | effect size | t-value | DF | SD |
|---|---|---|---|---|---|
| *low vs. high frequency exp.* | 0.0520 | 0.7236 | 1.9144 | 6 | 0.0021 |

**Table 4.3:** Context comparison: After-effect at threshold position. Results of paired t-test comparing the sum of the mean lateral deviation at threshold position of baseline trials that immediately followed CW and CCW curl force fields across experiments.

The p-value computed was slightly greater than the chosen threshold of 0.05. Therefore it could not be statistically proven that a difference exists in after-effect at the threshold position across contexts. However, because the p-value was very close to the threshold value and because the sample size used was small (n=7), we believed that there is in fact a statistically significant difference in after-effect between both contexts, even though it was not measured with the t-test.

Therefore, a second analysis of the after-effect was performed. Instead of only comparing the after-effect at the threshold position, the lateral deviation averaged over a time window of 0.2 seconds before the crossing of the threshold position was considered. This choice was based on the knowledge that the adaptation is best measurable in the beginning of reaching movements, as will be explained in the discussion in section 5.1.1. The average over time of the lateral deviation was computed for every baseline trial which immediately followed a curl force field trial. Next, the mean of these average lateral deviations was computed per participant, per direction of the preceding force field (CW or CCW) and per context. Based on these values, two variables were created.

$$X = \textit{mean average lateral deviation CCW} + \textit{mean average lateral deviation CW}$$
$$\textit{[low frequency exp.]}$$

$$Y = \textit{mean average lateral deviation CCW} + \textit{mean average lateral deviation CW}$$
$$\textit{[high frequency exp.]}$$

The following null hypothesis was tested:

$$H_0 : \textit{There is no statistically significant difference between the distributions of the variables } X \textit{ and } Y : \mu_X = \mu_Y.$$

The alternative hypothesis, which represents the hypothesis that is to be proven, was as follows:

$$H_a : \textit{There is a statistically significant difference between the distributions of the variables } X \textit{ and } Y : \mu_X > \mu_Y.$$

Because this alternative hypothesis is directed in a certain direction ($\mu_X > \mu_Y$) the paired t-test that was computed was one-tailed. The results obtained are summarized in table 4.4.

| **Paired t-test** | **p-value** | **effect size** | **t-value** | **DF** | **SD** |
|---|---|---|---|---|---|
| *low vs. high frequency exp.* | 0.0378 | 0.8111 | 2.1459 | 6 | 0.0010 |

**Table 4.4:** Context comparison: After-effect averaged over 0.2 s before crossing of threshold position. Results of paired t-test comparing sum of average lateral deviation over 0.2 seconds before crossing of the threshold position, of baseline trials following CW and CCW curl force field trials, across experiments.

The p-value obtained was smaller than the chosen statistically significant threshold of 0.05. The null-hypothesis was thus rejected and the alternative hypothesis confirmed. It was therefore proven that the after-effect, measured as the average deviation in the 0.2 seconds preceding the crossing of the threshold position, was greater in the low frequency experiment than in the high frequency experiment. The effect size was also computed using Cohen's d value. It was greater than 0.8, which is a big effect size, meaning that our results were reliable.

To better illustrate these results, the lateral deviation across all trials following CW and CCW curl field trials was illustrated for both experiments in figure 4.5. A clear difference in lateral deviation based on the context was noticeable, confirming our results.

### Between context changes in level of adaptation

Next, the level of adaptation to curl force field trials in each experiment was computed. It was evaluated by measuring the ratio of the after-effect due to a curl force field trial to

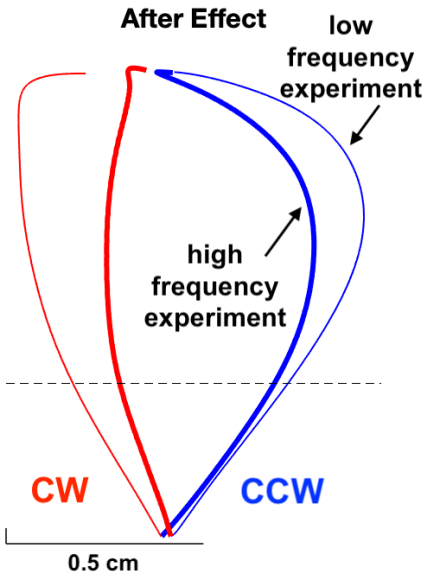


**Figure 4.5:** Context comparison: After-effect trajectories over time. Average across all baseline trials of a same experiment that immediately follow a curl force field of a same direction (CW - red or CCW - blue). Before computing the average across all participants, the lateral component of the average baseline trajectory was subtracted for each participant in each context, both for the CW and CCW curves.

the lateral deviation of that same curl force field trail. This ratio was computed for both experiments. The results obtained are gathered in table 4.5.

| | **Low frequency exp.** | **High frequency exp.** |
|---|---|---|
| **Level of adaptation $\sim$ k** | 0.2134 | 0.1725 |

**Table 4.5:** Context comparison: Level of adaptation to curl force field trials.

The levels of adaptation measured suggest that baseline trials of the low frequency experiment showed a 4% higher adaptation to curl force field trials than baseline trials of the high frequency experiment.

In this section we showed that the magnitude of the after-effect varied across contexts, suggesting that a perturbation experienced in the low frequency context had a larger impact on the next trial, indicating a larger adaptation. This was also shown by evaluating the rate of adaptation k, which was shown to be bigger in the low frequency experiment. The results will further be discussed in chapter 5.

## 4.2 Forward velocity

As explained in section 2.2.2, the forward velocity of the movement of the arm is a parameter that allows us to evaluate the control gains used by the robust controller. In this section we will present the different results obtained when measuring the forward hand velocity. We will start with the results obtained in the low frequency experiment, indicating how the forward hand velocity evolves within a block of trials. We will then present the results obtained

when comparing the forward hand velocity in both the low and high frequency experiments.

To analyse the evolution of the forward hand velocity across trials, baseline trials were given an index according to the number of perturbed trials, whichever the type, that immediately preceded the baseline trial. The labelling procedure is visible in figure 4.6. Throughout this section the same colour code as in figure 4.6 will be used to indicate trials of a certain index.

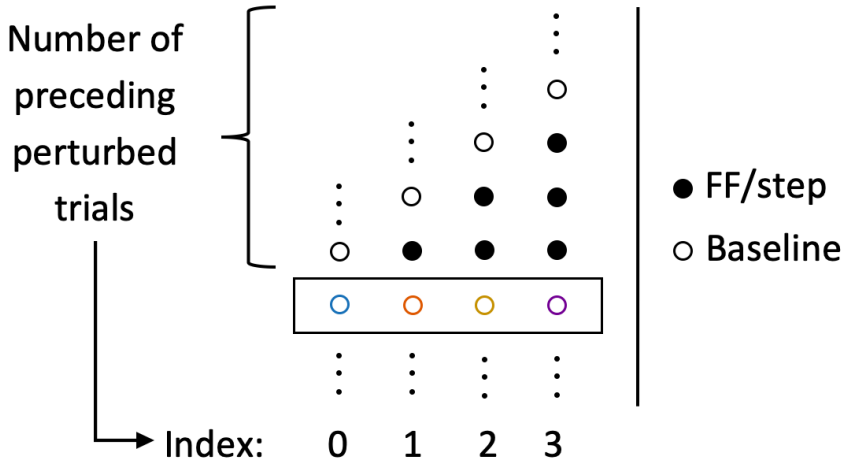


**Figure 4.6:** Labelling of baseline trials. Baseline trials were given an index based on the number of immediately preceding perturbations, whichever the type. Adapted from [8].

### 4.2.1 Trial-by-trial modulation

#### Low frequency experiment

The evolution of the forward hand velocity was first analysed across trials in the low frequency experiment. The forward hand velocity curves were averaged across trials of a same index and across participants. The different trials were aligned according to the position threshold, which is positioned at one third of the reaching movement, before being averaged. The time at which the threshold position was crossed was taken as origin for the time axis. The results are plotted in figure 4.7.

The results obtained showed a gradual increase in forward hand velocity at the threshold position for an increase in baseline trial index. These results were verified statistically by computing paired t-tests on the forward hand velocity at threshold position. Trials of index 0, 1 and 2 were compared, because not all participants experienced baseline trials of index 3. The results obtained are summarized in table 4.6.

The p-value computed when comparing the forward velocity at threshold position of trials of index 0 and trials of index 1 was lower than the 0.05 threshold. However, the p-value computed when comparing trials of index 1 and trials of index 2 was above this threshold. It was thus statistically proven that trials of index 1 showed a higher forward velocity at threshold position than trials of index 0, but no conclusions could be made on the difference in forward velocities at the threshold position between trials of index 1 and trials of index 2. However, the general tendency of increase in forward velocity linked to the increase in baseline index is clearly visible on figure 4.7.

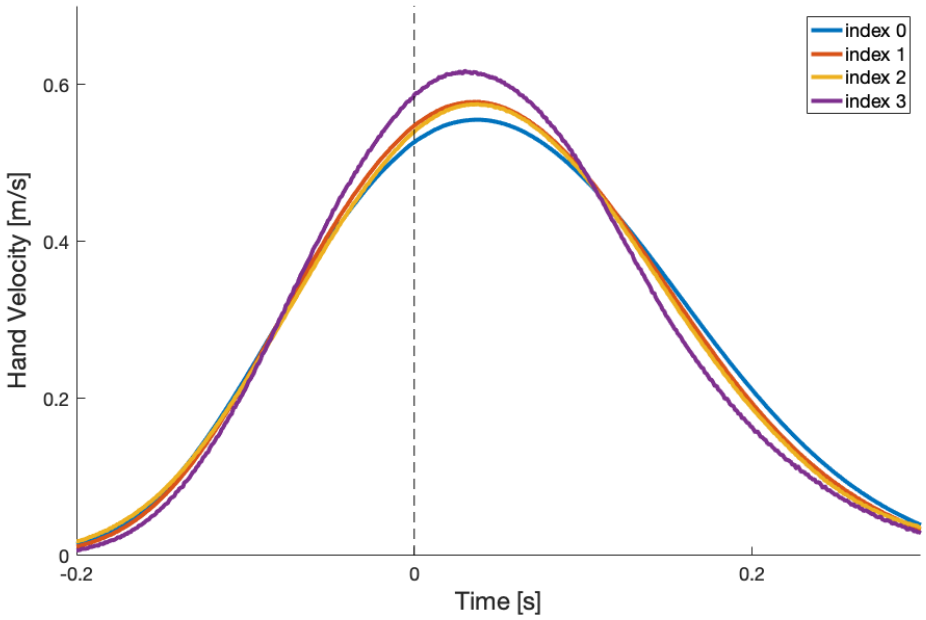


**Figure 4.7:** Trial-by-trial changes in forward hand velocity. Average across baseline trials of a same index and across participants, aligned according to the time at which they crossed the threshold position, which was defined as $t = 0$ [s]. The data of the low frequency experiment was used.

| Paired t-test | p-value | effect size | t-value | DF | SD |
|---|---|---|---|---|---|
| *Baseline trials: index 0 vs. index 1* | 0.0328 | 0.8495 | -2.2476 | 6 | 0.0227 |
| *Baseline trials: index 1 vs. index 2* | 0.3128 | 0.1943 | -0.5141 | 6 | 0.0409 |

**Table 4.6:** Trial-by-trial changes in forward hand velocity at threshold position. Results of paired t-test comparing the forward hand velocity at threshold position of baseline trials of index 0 and 1, and baseline trials of index 1 and 2. Data from the low frequency experiment.

### 4.2.2 Comparison across low and high frequency experiments

Next, the forward hand velocity was analysed across contexts. The average peak forward velocity was computed across baseline trials of a same index for each participant and in both contexts. The resulting curves are plotted in gray in figure 4.8. Next, the mean peak forward velocity across participants was computed and plotted in black in figure 4.8. The coloured dots correspond to the different baseline indexes, and correspond to the color-code established in figure 4.6.

In both the low and high frequency experiments, the peak forward velocity increased with an increase in baseline trial index, as predicted. Furthermore, the peak forward hand velocity seemed to be greater in the high frequency experiment than in the low frequency experiment. This hypothesis was confirmed by computing an ANOVA statistical test.

The data from figure 4.8 was used to compute the ANOVA test, i.e. the peak forward hand velocity of baseline trials of different indexes and contexts. However, because not all participants showed results for baseline trials of index 3 in the low frequency experiment, only baseline trials of index 0 through 2 were analysed. The ANOVA test tested the impact

of the baseline index and context on the forward hand velocity. The results obtained after sphericity corrections are gathered in table 4.7.

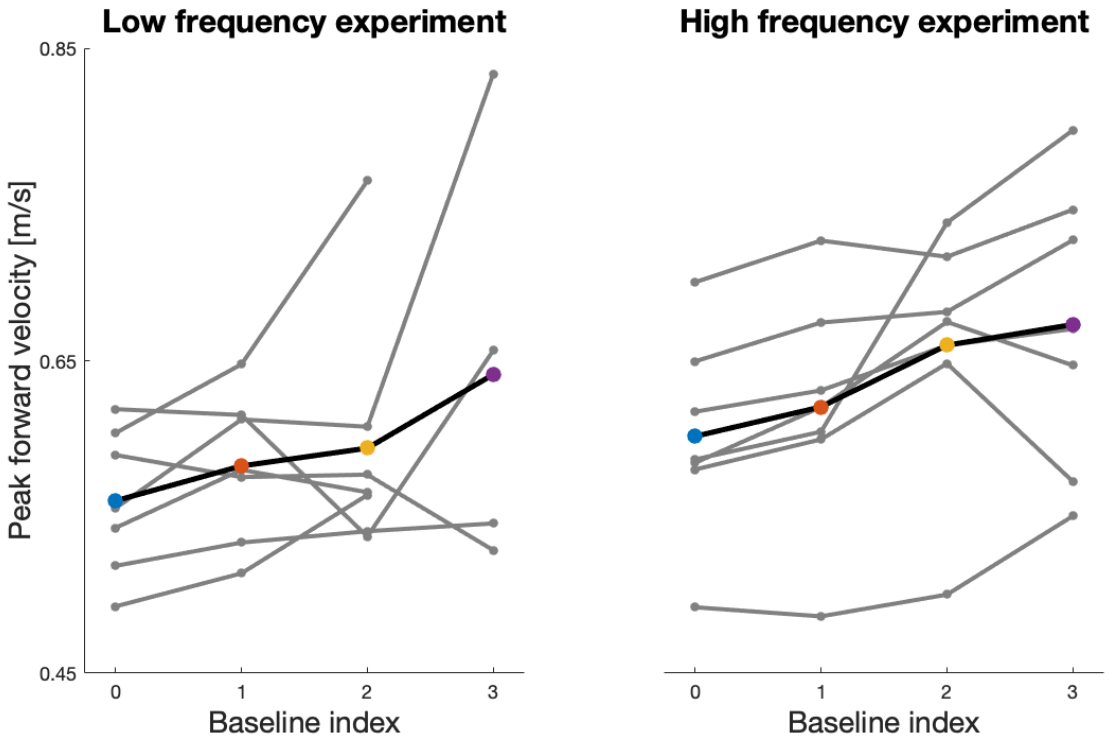


**Figure 4.8:** Context comparison: Peak forward hand velocity. Individual peak forward hand velocity as a function of baseline index (grey) per experiment. Peak forward hand velocities were then averaged across participants for each index (black). Colour code from figure 4.6 was used to illustrate average peak forward velocity for each index in both experiments.

| Effect | p-value | F-value |
|---|---|---|
| *Index* | 0.1284 | 2.9983 |
| *Context* | 0.0276 | 8.3600 |
| *Context : Index* | 0.4194 | 0.8034 |

**Table 4.7:** Context comparison: Peak forward hand velocity. Results of ANOVA test on the peak forward velocity during baseline trials of index 0, 1 and 2 of the low and high frequency experiments.

The p-value indicating the index's influence on the forward hand velocity was greater than the statistically significant threshold of 0.05. It could thus not be proven that the index influences the forward velocity during baseline trials. The p-value indicating the context's influence on the forward hand velocity was lower than the statistically significant threshold of 0.05. This indicates that the distribution of the forward hand velocity is statistically different in both contexts. More specifically, the peak forward hand velocity is on average greater in the high frequency experiment than in the low frequency experiment. The joint p-value of both the context and the index of a trial was also computed and it was significantly above the 0.05 threshold, indicating that there is no particular relationship between the context and index of a trial when measuring peak forward velocities.

To illustrate these results, figure 4.9 plots the peak forward hand velocity distribution with a 95 % confidence interval, both as a function of the baseline index (left-hand figure) and as a function of the experiment (right-hand figure).

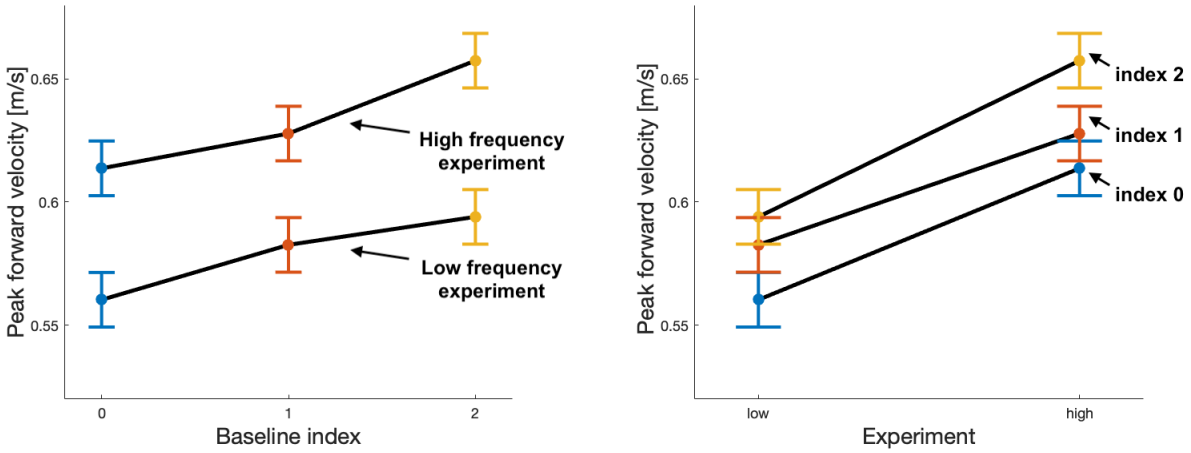


**Figure 4.9:** Context comparison: Peak forward hand velocity statistical distribution. 95 % confidence interval of mean peak forward velocity as a function of baseline index (left-hand side) and as a function of the context (right-hand side).

It is indeed clear that a real difference in forward velocity between both experiments exists (figure 4.9 left-hand side) and that the difference in forward velocity is less noticeable between indexes (figure 4.9 right-hand side). However, when analysing figure 4.9, it is clear that baseline trials of index 0 and index 2 have a clear difference in distributions. A paired t-test was thus computed on the peak forward velocity of trials of index 0 and trials of index 2. That is, for each participant and in each context, two values were computed, corresponding to the average peak forward velocity across trials of index 0 and 2. These two values were then compared using a paired t-test. The results are gathered in table 4.8.

| **Paired t-test** | **p-value** | **effect size** | **t-value** | **DF** | **SD** |
|---|---|---|---|---|---|
| *Baseline trials: index 0 vs. index 2* | 0.0125 | 0.8856 | -2.5312 | 13 | 0.0572 |

**Table 4.8:** Trial-by-trial changes in peak forward hand velocity. Results of paired t-test comparing the peak forward hand velocity of baseline trials of index 0 and 2. Data from the low and high frequency experiment.

The p-value computed was lower than the 0.05 threshold, indicating that the peak forward velocity is indeed greater during baseline trials of index 2 than during baseline trials of index 0, both in the low and high frequency experiments.

Next, figure 4.8 was slightly modified to illustrate the differences in relative variation of the peak velocity between indexes. This was done by subtracting the mean peak forward velocity across indexes per participant. The resulting plots are visible in figure 4.10, and allow us to compare the peak velocity variations independent of any differences in sample means.

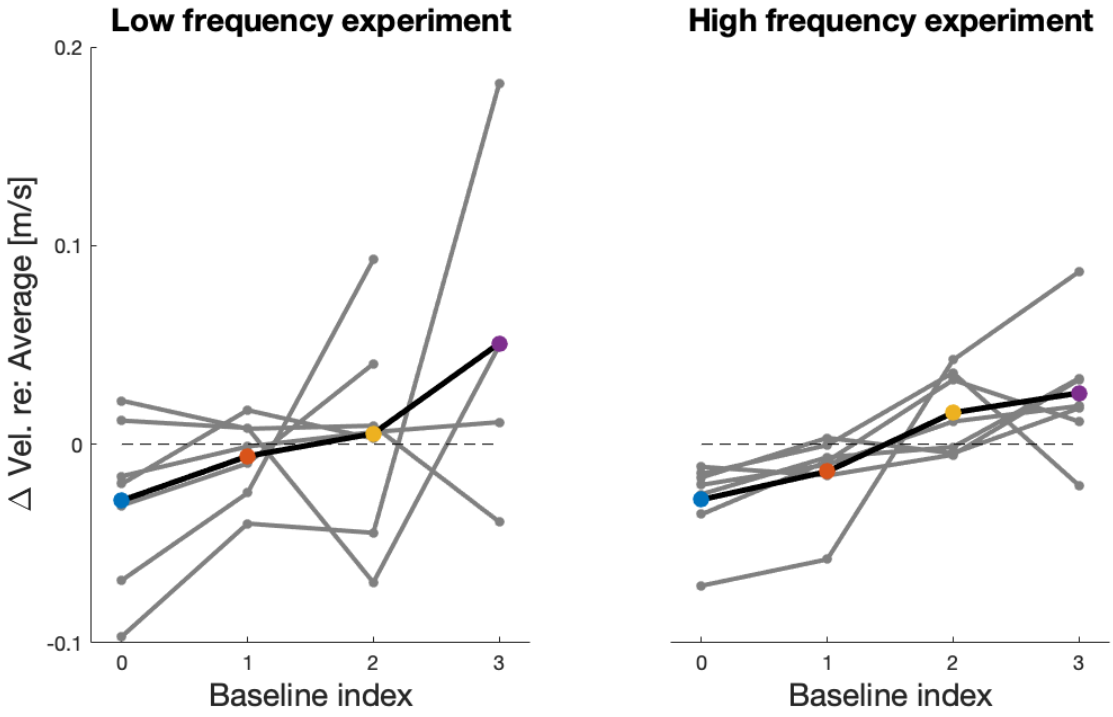


**Figure 4.10:** Context comparison: Relative peak forward hand velocity. Individual peak forward hand velocity as a function of baseline index (grey) per experiment. Individuals' average across baseline indexes was subtracted per participant, to obtain relative peak forward velocity. Relative peak forward hand velocities were then averaged across participants for each index (black). Colour code from figure 4.6 was used to illustrate average relative peak forward velocity for each index in both experiments.

These plots illustrate how the peak velocity evolved as a function of the baseline index for each participant. In both experiments, a clear increase in peak forward velocity was measured. The increase in peak forward velocity seemed less variable from participant to participant in the high frequency experiment than in the low frequency experiment. Indeed, the increase of peak velocity of each individual seemed very similar to the mean increase across participants in the high frequency experiment. In the low frequency experiment, the increase in peak velocity across indexes seemed less constant across participants.

To evaluate the differences in relative variation of the peak velocity, a levene test was computed [22]. The levene test was used to determine whether the variance of the relative peak forward hand velocity curves was the same in both experiments. The results obtained are gathered in table 4.9.

| **Effect** | **p-value** | **F-value** |
|---|---|---|
| *Context* | 0.0918 | 2.9834 |

**Table 4.9:** Context comparison: Relative peak forward hand velocity. Results of levene test on the homogeneity of variances of the relative peak forward velocity during baseline trials of index 0, 1 and 2 of the low and high frequency experiments.

The p-value computed was greater than the 0.05 threshold. It could therefore not be statistically proven that a difference in distribution exists between both experiments. However, even though the p-value obtained was bigger than the chosen threshold of 0.05,

it remains quite small ($< 0.1$). Therefore, it could be that the results were not significant enough due to the small sample size used, and that a true difference in variance exists between both experiment.

In this section we showed that the magnitude of the peak forward hand velocity varied across contexts; higher peak forward velocities were measured during baseline trials of the high frequency experiment than during baseline trials of the low frequency experiment. These results suggest that the control gains of the robust controller were on average higher in the high frequency experiment, indicating that a more robust strategy was used. These results will be further discussed in chapter 5.

## 4.3 Robustness

As explained in section 2.2.2, the increase in control gains can be measured by an increase in robustness in responses to perturbations. Indeed, it was demonstrated in the 2019 paper on robust control that a robust controller can produce higher control gains to reduce the impact of external perturbations on the hand trajectory. More precisely, hand trajectories of responses to perturbations which occurred "early", as will be defined in section 4.3.1, were noticed to be less sensitive to external disturbances, indicating changes in control gains. In this section we will analyse the robustness of responses to perturbations, which we define as the sensitivity of the hand trajectory to external disturbances, to measure these changes in control gains. The deviation of the hand path during perturbations will be measured to quantify the sensitivity of the hand trajectories. The changes in robustness measured will enable us to learn more on the changes in control strategy used by the controller.

We will start by analysing the within context changes in robustness of responses to perturbations and finish with a between context analysis.

### 4.3.1 Trial-by-trial modulation

To analyse the trial-by-trial changes in robustness of responses to perturbations, perturbed trials were classified into two categories, early and late trials. The categorization into both categories is illustrated in figure 4.11. Trials were first given an index based on the number of immediately preceding baseline trials. Based on this index, perturbation trials were separated into both categories. The split between early and late perturbations was made at the median of the perturbation indexes, which was equal to 3 for the low frequency experiment and 1 for the high frequency experiment.

#### Low frequency experiment

Once all the curl force field trials of the low frequency experiment were classified in one of both groups, early and late perturbations, the average hand path across trials of a same group (early or late) and same direction (CW or CCW) was made. All trials were aligned according to the threshold position before being averaged. The results obtained are illustrated in figure 4.12. The hand paths of early curl field trials seemed to be less

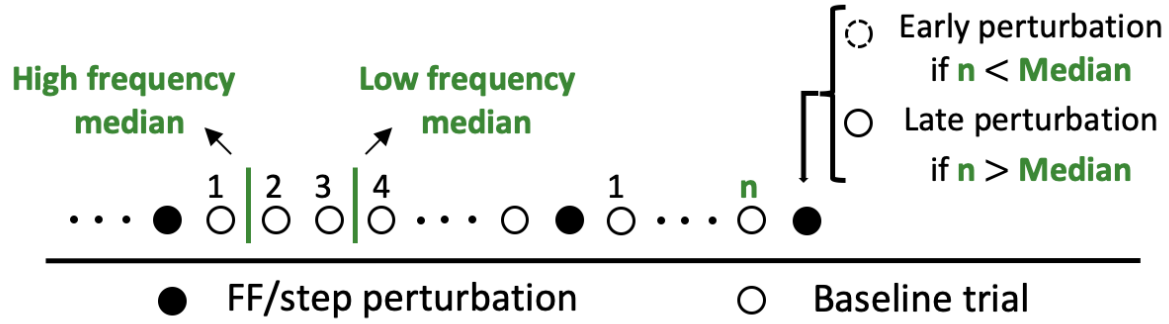


**Figure 4.11:** Classification of perturbation trials. Perturbation trials were classified as early or late trials, according to their occurrence relative to the last perturbation trial. The split between both categories was made according to the median number of baseline trials between two perturbation trials. If a perturbed trial occurred after more than this median number of baseline trials, it was classified as late, else it was classified as early. The median number of baseline trials between two perturbation trials was equal to 1 in the high frequency experiment and 3 in the low frequency experiment.

deviated than the ones of late curl field trials, indicating that a more robust strategy is used right after a perturbation.

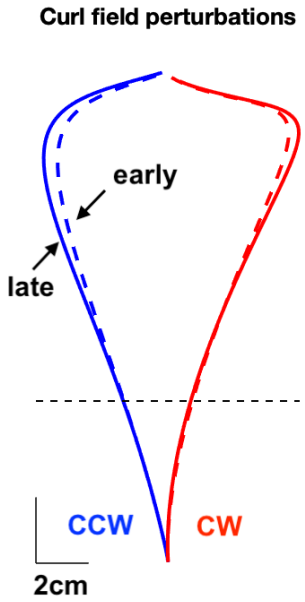


**Figure 4.12:** Trial-by-trial changes in robustness: Low frequency experiment. Average across early (dashed) and late (full), CCW (blue) and CW (red) curl field trials of all participants.

### High frequency experiment

Once all perturbed trials of the high frequency experiment were classified, the average hand path across trials was plotted for all three perturbation types in both directions and both for late and early trials. The results are visible in figure 4.13.

Once again, a difference between late and early trials was noticeable. This difference was particularly clear for step-load trials. Early trials that encountered deviations were less

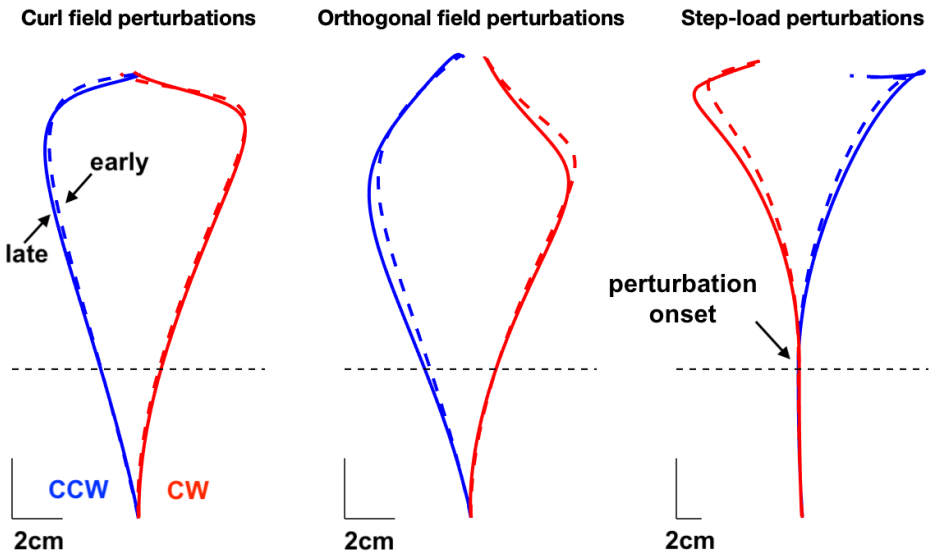


**Figure 4.13:** Trial-by-trial changes in robustness: High frequency experiment. Left: CCW (blue) and CW (red) curl field trials. Middle: Leftward (blue) and rightward (red) orthogonal field trials. Right: Leftward (red) and rightward (blue) step-load trials. Average across early (dashed) and late (full) trials of all participants.

perturbed than late trials, indicating that the control gains of the robust controller are increased after a perturbation, and decreased after each baseline trial.

### 4.3.2 Comparison across low and high frequency experiments

Next, a comparison across contexts of the lateral deviation during curl field trials was performed. The average across participants of the hand path during curl field trials was computed for both contexts and both directions. The results are visible on figure 4.14.

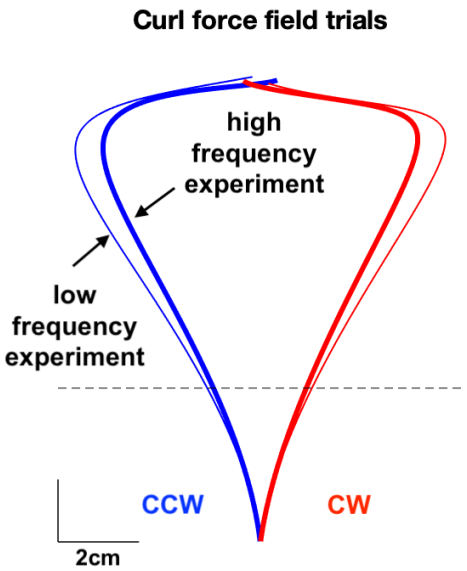


**Figure 4.14:** Context comparison: Robustness to curl force field trials. Average across all CCW (blue) and CW (red) curl field trials of all participants in the low (thin) and high (thick) frequency experiments.

The hand paths from the low frequency experiment were more deviated than the ones from the high frequency experiment. To confirm these results, a comparison across contexts of the maximum lateral deviation during curl force field trials was performed. The results are visible on figure 4.15.

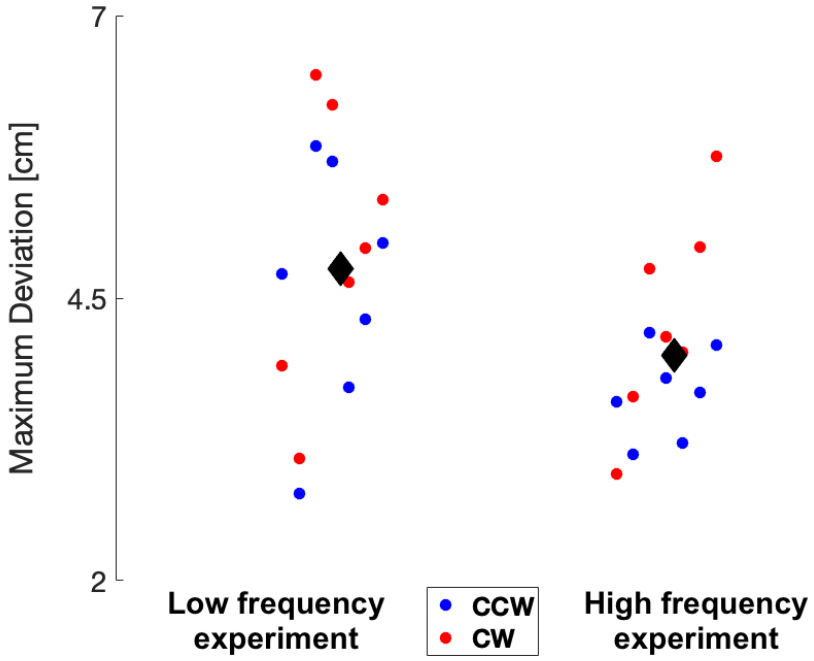


**Figure 4.15:** Context comparison: Maximum lateral deviation during curl force field trials. The maximum lateral deviation during curl force field trials of a same direction was averaged per participant and per experiment. A grand average across participants was computed per experiment (black diamond).

The mean maximum deviation, represented by a black diamond in figure 4.15 was indeed greater in the low frequency experiment than in the high frequency experiment. To confirm this hypothesis statistically, a paired t-test was computed on the maximum deviation during curl field trials of the low and high frequency experiments. The two variables compared were the following:

$$X = \textit{Maximum lateral deviation during curl field trials (CW and CCW).} \\ \textit{[low frequency exp.]}$$

$$Y = \textit{Maximum lateral deviation during curl field trials (CW and CCW).} \\ \textit{[high frequency exp.]}$$

Both variables had two values per participant, associated to the mean maximum lateral deviation of CW and CCW curl force field trials. X and Y represent two measurements of the same sample, i.e the maximum deviation participants experienced in both contexts. The null hypothesis tested was the following:

$$H_0 : \textit{There is no statistically significant difference between the distributions of the variables } X \textit{ and } Y : \mu_X = \mu_Y.$$

The alternative hypothesis, which represents the hypothesis that is to be proven, was as follows:

$$H_a : \textit{There is a statistically significant difference between the distributions of the variables } X \textit{ and } Y : \mu_X > \mu_Y.$$

Because this alternative hypothesis is directed in a certain direction ($\mu_X > \mu_Y$) the paired t-test that was computed was one-tailed. The results obtained are gathered in table 4.10.

| **Paired t-test** | **p-value** | **effect size** | **t-value** | **DF** | **SD** |
|---|---|---|---|---|---|
| *Curl FF: low vs. high frequency exp.* | 0.0028 | 0.8856 | 3.3136 | 13 | 0.0087 |

**Table 4.10:** Context comparison: Maximum lateral deviation during curl force field trials
Results of a one tailed paired t-test on maximum lateral deviation during curl force field trials of the low and high frequency experiment.

The p-value obtained was smaller than the chosen statistically significant threshold of 0.05. The null-hypothesis was thus rejected and the alternative hypothesis confirmed. It was proven that the maximum deviation due to curl force field perturbations was greater in the low frequency experiment than in the high frequency experiment. The effect size was also computed using Cohen's d value and was larger than 0.8, which is considered to be a large effect size. The results were thus considered reliable despite the small sample size.

In this section we showed that the magnitude of the lateral deviation experienced during curl force field trials varied across contexts; the hand trajectory of subjects seemed to be less impacted by curl force field trials in the high frequency experiment than in the low frequency experiment. These results suggest that the control gains of the robust controller were higher on average in the high frequency experiment, indicating that a more robust controller was used. These results will be further discussed in chapter 5.

## 4.4 Co-contraction

As explained in section 2.2.2, it was noticed in the 2019 paper on robust control that a correlation exists between the increase in control gains, measurable by the increase in speed and robustness to responses, and the co-contraction of the pectoralis major and posterior deltoid. This correlation suggests that the co-contraction of both muscles could be involved in the modulation of the control gains.

In this section we will analyse the modulation of co-contraction, to confirm this hypothesis. We will start by analysing the trial-by-trial changes in the high frequency experiment, and we will then analyse the changes in co-contraction across contexts.

### 4.4.1 Trial-by-trial modulation

To analyse the trial-by-trial changes in co-contraction, force field trials were given an index based on the number of immediately preceding baseline trials, and were separated into two categories : early trials and late trials. This categorization is the same categorization

as the one described in section 4.3 and illustrated by figure 4.11. The high frequency experiment will be considered to analyse the trial-by-trial changes.

### High frequency experiment

The muscle activity of both muscles was measured during early and late step-load trials. Figure 4.16 illustrates the muscle activities of both muscles, both for leftwards and rightwards step-load perturbations.

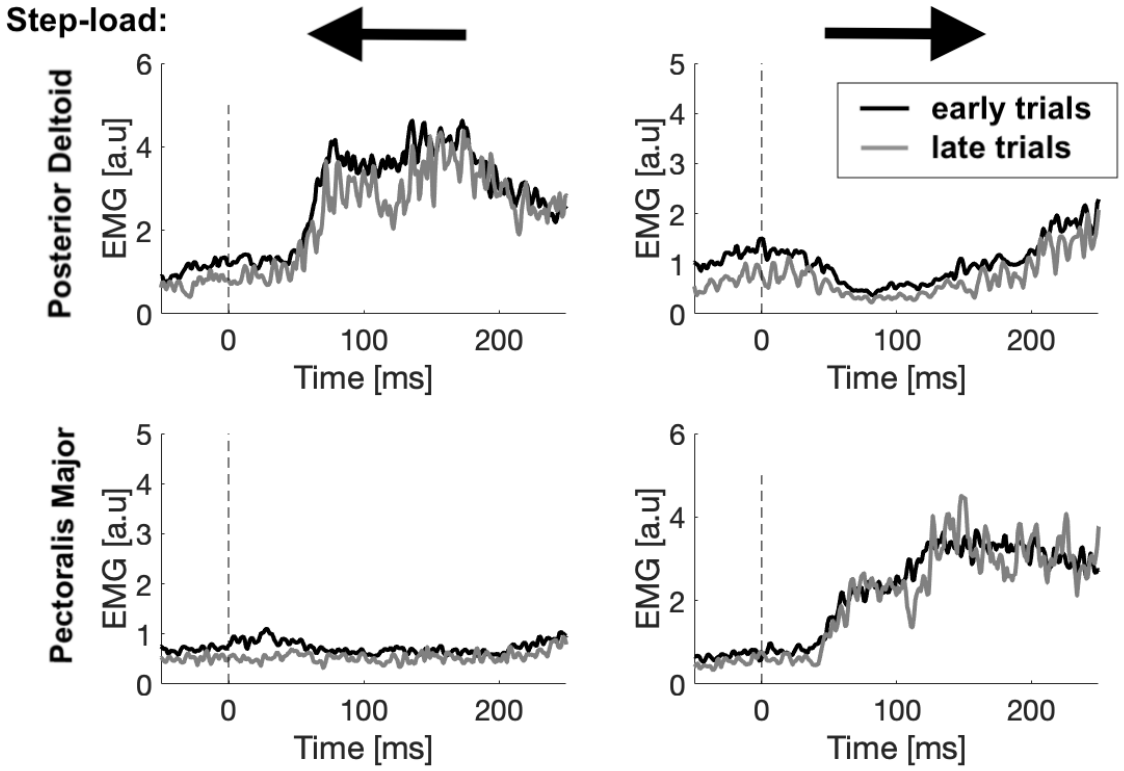


**Figure 4.16:** Trial-by-trial modulation of the muscle responses to perturbations. Muscle responses to leftward (left-hand side) and rightward (right-hand side) step-load trials. Muscle activities were averaged both for the posterior deltoid (top) and pectoralis major (bottom) muscles across all early (black) and across all late (grey) trials. Muscle activities correspond to the EMG data normalized using the calibration trials as explained in section 3.3.

As predicted, the muscle activity of early trials was higher for both muscles and in both cases (leftwards of rightwards step-load perturbations) than the muscle activity of late trials. This confirms the hypothesis that the co-contraction of both muscles increases right after a perturbation, to increase the control gains.

These results were verified statistically by computing an ANOVA test on the average muscle activity during the 50 ms before the crossing of the position threshold. The ANOVA results are gathered in table 4.11. A p-value inferior to the threshold value of 0.05 was computed, indicating that there is indeed a difference in muscle activity between late and early trials.

| Effect | p-value | F-value |
|---|---|---|
| *Category* | 0.0059 | 17.2455 |

**Table 4.11:** Trial-by-trial changes in muscle activity during step-load trials. Results of ANOVA test comparing muscle activities averaged over 50 ms before the crossing of the threshold position of early and late step-load trials. Muscle activities correspond to the EMG data normalized using the calibration trials as explained in section 3.3

### 4.4.2 Comparison across low and high frequency experiments

Next, the changes in co-contraction were measured across experiments. This was first done for all baseline trials, and then for perturbation trials.

#### Muscle activity during baseline trials

The average muscle activity across baseline trials of both the pectoralis major and posterior deltoid muscles was plotted for each participant and for both experiments in figure 4.17.

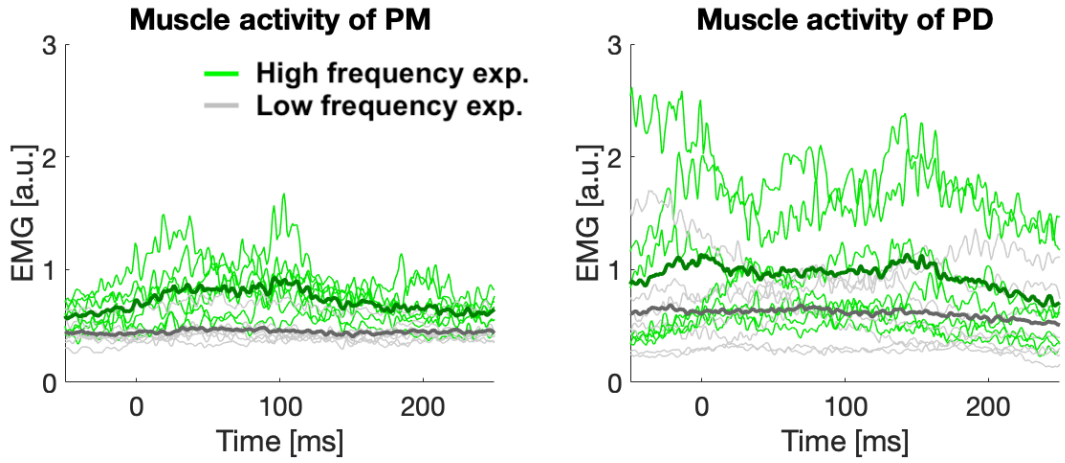


**Figure 4.17:** Context comparison: Muscle activity during baseline trials. Average muscle activity of PM (left-hand side) and PD (right-hand size) muscles across all baseline trials of the low (grey) and high (green) frequency experiments per participant (light) and across participants (dark). Muscle activities correspond to the EMG data normalized using the calibration trials as explained in section 3.3.

A clear difference was noticeable between the muscle activities in both experiments. As predicted, the baseline muscle activity was higher in the high frequency experiment than in the low frequency experiment.

To confirm this hypothesis statistically, an ANOVA test was computed. Baseline trials were sorted according to the number of immediately preceding curl field trials, as described by figure 4.1. Three categories of trials were considered for this analysis: baseline trials of index 0, baseline trials of index 1 preceded by a CW curl field trial, and baseline trials of index 1 preceded by a CCW curl field trial. The mean muscle activity of both muscles during the 50 ms that preceded the threshold position was computed for all baseline trials in both experiments. This mean muscle activity was then averaged across trials of a same category for each muscle, subject and context. The analysed effects of the ANOVA test

were the baseline trial's index and context. The results obtained are gathered in table 4.12.

| Effect | p-value | F-value |
|---|---|---|
| *Index* | 0.0037 | 21.1191 |
| *Context* | 0.0317 | 7.7690 |
| *Context : Index* | 0.0897 | 4.0881 |

**Table 4.12:** Context comparison: Muscle activity during baseline trials. Results of ANOVA test comparing muscle activities of baseline trials of index 0, trials of index 1 following CW curl force field trials and trials of index 1 following CCW curl force field trials, both for the low and high frequency experiment. Muscle activities correspond to the EMG data normalized using the calibration trials as explained in section 3.3, and were averaged over the 50 ms before the crossing of the threshold position.

The p-value indicating the index's influence on the muscle activities was lower than the statistically significant threshold of 0.05, indicating that the index of the baseline trial influences the muscle activity of both muscles. Furthermore, the p-value indicating the context's influence on the muscle activities was also lower than the statistically significant threshold of 0.05. It was thus proven that the context, represented by the low and high frequency experiments, also impacts the muscle activities.

### Muscle activity during curl force field trials

The muscle activity of both muscles across experiments was also compared during curl force field trials. The muscle activity of both muscles was plotted during CW and CCW curl force field trials for both experiments. The results obtained showed higher muscle activities in the high frequency experiment than in the low frequency experiment, as shown in figure 4.18.

To confirm these results statistically, a paired t-test was performed on the average muscle activity of both muscles during the 50 ms before the crossing of the threshold position during curl force field trials. The results of the paired t-test are gathered in table 4.13.

| Paired t-test | p-value | effect size | t-value | DF | SD |
|---|---|---|---|---|---|
| *Curl FF: low vs. high frequency exp.* | 0.00005 | 0.8624 | -4.5634 | 27 | 0.2512 |

**Table 4.13:** Context comparison: Muscle activity during curl force field trials. Results of one tailed paired t-test comparing the muscle activities during curl force field trials averaged of 50 ms before the crossing of the threshold position of the low and high frequency experiments. Muscle activities correspond to the EMG data normalized using the calibration trials as explained in section 3.3.

The p-value obtained was well below the threshold value of 0.05, indicating that a difference exists between the muscle activity before the crossing of the threshold position during curl field trials of the low and high frequency experiments. Furthermore, the effect size computed was above 0.8 indicating that the results are reliable.

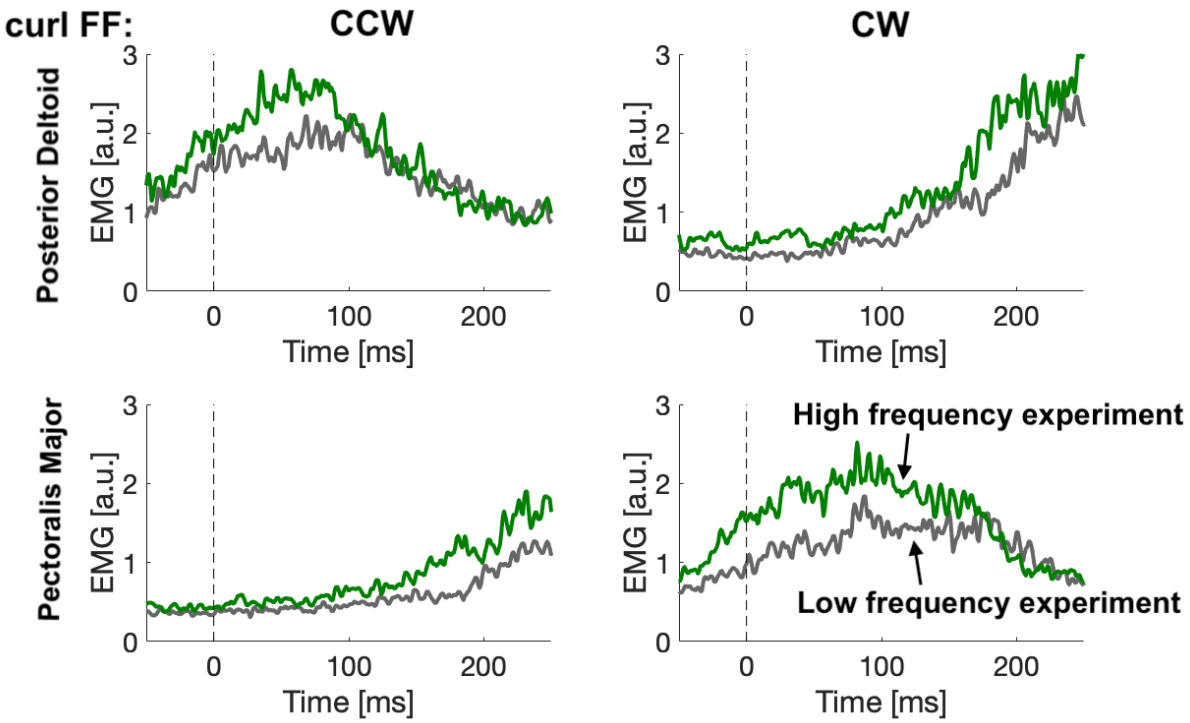


**Figure 4.18:** Context comparison: Muscle activity during curl force field trials. Average muscle activities across CCW (right-hand side) and CW (left-hand side) curl force field trials of the PD (top) and PM (bottom) muscles both for the low (grey) and high (green) frequency experiments. Muscle activities correspond to the EMG data normalized using the calibration trials as explained in section 3.3.

In this section we showed that the muscle activities of the pectoralis major and posterior deltoid varied across contexts. Higher muscle activities were measured in the high frequency experiment, suggesting that the co-contraction of both muscles is used to increase the control gains and obtain a more robust controller.

# Chapter 5

# Discussion

In this section we will discuss the results obtained in section 4. We will start with a within context analysis of the results, followed by an across contexts analysis.

## 5.1 Modulation of control strategy within contexts

### 5.1.1 After-effect

The within context modulation of the after-effect was studied for the low frequency experiment in section 4.1.1. Baseline trials were given an index based on the number of immediately preceding curl field trials of a certain direction, as illustrated in figure 4.1. The results were plotted in figure 4.3, and matched our predictions. The after-effect, which represents the lateral deviation that occurs in the opposite direction of an experienced force field after removal of that force field, was proportional to the baseline index. Indeed, baseline trials that followed two successive curl force field trials of a same direction were more deviated at the threshold position than baseline trials that followed a single curl force field trial.

However, an observation was made. It was noticed that during the second half of reaching movements, the average after-effect hand paths across trials of index 1 and trials of index 2 following counter-clockwise curl force field trials, crossed each other. Thus, the lateral deviation of the hand path of trials of index 2 became smaller than the lateral deviation of the hand path of trails of index 1 at the end of their reaching movements, as illustrated in figure 5.1.

However, this change in relationship between trials of index 1 and 2 which occurred at the end of reaching movements does not question the changes in after-effect that were discovered between these two categories of trials. Indeed, it could be that this change of relationship was simply due to the small sample size that was used and that it does not illustrate the true relationship between hand paths of trials of index 1 and trials of index 2. Furthermore, a second probable explanation to this phenomenon could be based on the activation of the feedback mechanism which occurs later on in the movement. It could be that the hand paths of trials of index 2 are more deviated in their first half, due to adaptation, but are then strongly corrected by online feedback, reducing the lateral deviation of the hand path at the end of the trial.

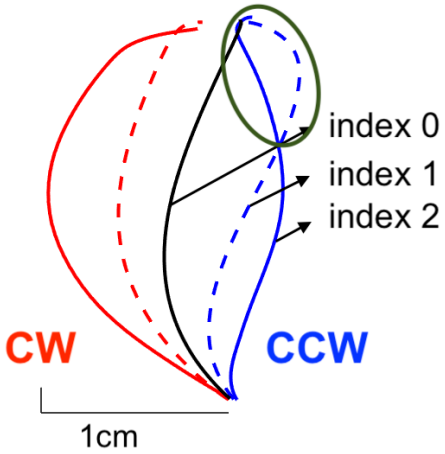


**Figure 5.1:** Observation : Trial-by-trial changes in after-effect. Crossing of the hand trajectories of baseline trials of index 1 and 2 following CCW curl force field trials. Data from the low frequency experiment.

These results highlight the importance of measuring the after-effect early on in reaching movements, to correctly capture the impact of adaptation on the hand paths. Therefore, the after-effect of trials of index 1 and trials of index 2 was compared at the threshold position using a paired t-test. The results obtained, gathered in table 4.1, showed that the after-effect was truly bigger during trials of index 2 than trials of index 1.

It was thus proven that an increase in baseline index leads to an increase in after-effect, indicating that the controller adapts its internal representation after each perturbation. The adaptation of the internal representation can be modelled by the following equation, as described in section 2.2.1 :

$$A' = A + k * \Delta A \tag{5.1}$$

where k represents the level of adaptation. This model of adaptation using a variable k indicating the level of adaptation does not fully represent the true working of the nervous system but it is useful to quantify motor learning. Indeed, k is used to represent the rate of adaptation, i.e. the percentage of adaptation to the experienced disturbance. We decided to quantify this value to estimate the rate of adaptation in the low frequency experiment.

### Quantification of the level of adaptation k

In a standard context, k is expected to be equal to a value between 0 and 1, representing a situation in between a context with no adaptation at all and a context in which the internal model is fully adapted according to the experienced disturbance. However, some people are only capable of adapting their internal representation to some extent. It was for instance shown that patients with cerebellar dysfunction tend to experience a failure in motor skill learning [21].

The level of adaptation was quantified by computing the ratio of the after-effect due to a curl force field trial to the lateral deviation of the hand path during that same curl force field trial. Both values were extracted at threshold position and the ratio was averaged

across baseline trials of a same index. Two values were obtained, a ratio representing the level of adaptation experienced by baseline trials of index 1 and a ratio representing the level of adaptation experienced by baseline trials of index 2 . For baseline trials of index 2, the lateral deviation of the hand path of the baseline trial was divided by the lateral deviation of the first of the two preceding curl force field trials. Therefore, both ratios illustrated to which extent the controller was adapted to the experienced force field, after having experienced it once or twice in a row.

The results, gathered in table 4.2, showed that on average baseline trials of index 1 showed a 20.1% adaptation to the experienced curl force field whereas trials of index two showed a 39.2% adaptation to the experienced curl force field. Baseline trials of index 2 where thus twice as adapted as baseline trials of index 1.

These changes in adaptation can be explained by equation 5.1. After a single perturbation, the internal model of the movement dynamics was only partially adapted, according to the rate of adaptation k which was estimated to be equal to 20%. After a second perturbation of the same sort, the internal model was once again adapted, this time to the second perturbation according to a certain percentage k'. The build up of these two successive adaptations led to hand paths which were shown to have experienced a 40% adaptation to the original perturbation. This suggested that the rate of the second adaptation, defined as k', was also equal to 20%, as the build of two adaptations of 20% leads to an adaptation of 40%. It is this phenomenon that explains the results visible on figure 4.3, indicating that the after-effect is larger for baseline trials of index 2.

These results suggest that throughout the low frequency experiment, the trial-by-trial level of adaptation k was constant and of about 20%. For baseline trials of index 2, it was the build up of two successive adaptations that led to bigger after-effects, and not a change in level of adaptation.

### 5.1.2 Forward velocity

The within context modulation of the forward hand velocity was studied for the low frequency experiment. We chose to specifically analyse the forward hand velocity as it was shown in the 2019 paper on robust control that changes in forward hand velocity did not correlate with changes in after-effect [8]. Indeed, the lateral deviation following perturbation trials decreased back to baseline levels earlier on than the forward hand velocity. This suggests that the changes in forward velocity were not correlated with the changes in adaptation, and were therefore a sign of another change in strategy, towards a more robust controller.

Baseline trials of the low frequency experiment were given an index based on the number of immediately preceding perturbations, whichever the type, as illustrated in figure 4.6. The forward hand velocity across trials of a same index was plotted in figure 4.7. An increase in forward velocity was noticeable around the threshold position for trials of a higher index, as was predicted by the results of the 2019 paper on robust control. This increase in forward hand velocity was statistically proven between trials of index 0 and trials of index 1, but could not be proven between trials of index 1 and 2. Indeed, the difference in

forward velocity was less noteworthy between trials of index 1 and 2, and could not be proven with the small data size of 7 subjects which was used. The difference in forward velocity at threshold position was once again very clear between trials of index 2 and trials of index 3, but no statistical test was computed to prove this as not all participants experienced baseline trials of index 3.

Altogether, a clear increase in forward velocity at threshold position was noticeable for an increase in baseline trial index. As explained in section 2.2.2, the forward hand velocity is a variable used to measure the changes in control gains. Therefore, the increase in forward velocity measured for higher baseline indexes suggests that the control gains of the controller are increased after a perturbation, and that a build up occurs after a series of successive perturbation trials.

### 5.1.3 Robustness

The robustness of responses to perturbations was analysed both for perturbations of the low frequency experiment and high frequency experiment. Trials were classified into two categories, late and early trials, according to whether they occurred before or after the median number of baseline trials between two perturbation trials, as illustrated in figure 4.11. The median was equal to 3 for the low frequency experiment and 1 for the high frequency experiment, which is consistent with the fact that perturbations were more frequent in the high frequency experiment.

A global difference was noticeable between the early and late trials of both the low and high frequency experiments, as shown in figure 4.12 and 4.13. Early trials were less deviated by the same perturbations. No significant statistical tests could be computed for this section because of the small data size used, but our results were confirmed by the results presented in the 2019 paper on robust control, which were similar.

These results suggest that during both experiments, the controller was more robust during early trials than late trials, indicating that the control gains are increased after a perturbation and that they then decrease after a sequence of baseline trials.

### 5.1.4 Co-contraction

The within context modulation of co-contraction was studied during the high frequency experiment. Step-load trials were classified as late or early trials according to their occurrence relative the median number of baseline trials between two perturbations, as illustrated in figure 4.11.

Figure 4.16 illustrates the average muscle activity across trials of a same category, early or late trials, for both muscles and for both leftward and rightward step-load trials. In all four cases, the muscle activity was shown to be greater for early trials, indicating that an increase in co-contraction occurs after a perturbation, and that the levels of muscle activity are then decreased after a sequence of baseline trials. These results were verified statistically using an ANOVA test.

These changes in muscle activity confirm our predictions described in section 2.2.2. The

co-contraction of the pectoralis major and posterior deltoid is used by the CNS to increase the control gains of the controller, making it more robust to perturbations. Higher muscle activities were measured during early trials, indicating that the muscle co-contraction is increased right after a perturbation to increase the control gains of the controller. The muscle activities then decrease when faced with a sequence of baseline trials, gradually lowering the control gains back to baseline levels.

## 5.2 Modulation of control strategy across contexts

In this section we will discuss the results obtained when comparing the low and high frequency experiments, which was the main objective of this master thesis. We will discuss the results presented in section 4.

As predicted by the 2019 paper on robust control, the results showed changes in adaptive and robust control across experiments. By analysing figures 4.14 and 4.5, which were plotted side-by-side in figure 5.2 for clarity, these changes in adaptive and robust control are visible. The left-hand side plot illustrates the robustness of responses to curl force fields and the right-hand side plot illustrates the after-effect present in baseline trials following these curl force field trials.

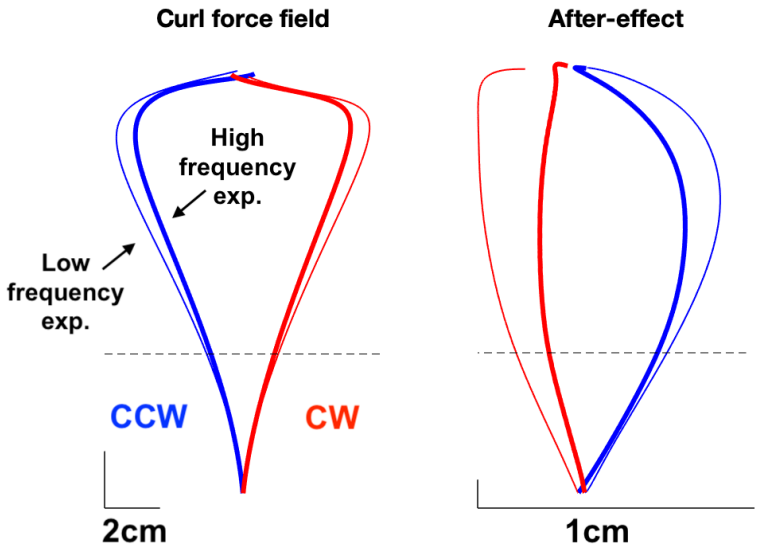


**Figure 5.2:** Context comparison: Robustness and after-effect. Left-hand side. Average lateral deviation during CCW (blue) and CW (red) curl force field trials of the high (thick) and low (thin) frequency experiments. Right-hand side. Average lateral deviation during baseline trials that immediately followed CCW (blue) and CW (red) curl force field trials in the high (thick) and low (thin) frequency experiments.

When analysing the robustness of responses to perturbations, plotted in the left-hand side of figure 5.2, trials of the high frequency experiment seemed to be more adapted. Indeed, the lateral hand deviation during curl field trials was smaller during the high frequency experiment than during the low frequency experiment.

However, when analysing the after-effect in both experiments, this suggestion was contradicted. Hand paths of baseline trials following curl force field trials were more deviated in the low frequency experiment than in the high frequency experiment. The increase in after-effect measured in the low frequency experiment suggests that subjects were more adapted to curl force fields in the low frequency experiment, and not in the high frequency experiment as suggested earlier. The smaller lateral deviation during curl force field trials of the high frequency experiment is therefore not related to a change in adaptation. It can rather be explained by a change in robustness of the controller, due to an increase in control gains as explained in section 2.2.2.

Altogether, the results obtained suggest that a more robust controller is used in a less predictable environment. Simultaneously, our results predict a decrease in adaptation when switching to a less predictable environment. These findings will further be described by discussing each parameter that was analysed separately.

### 5.2.1 After-effect

The between contexts modulation of the after-effect was studied in section 4.1.2. By performing a t-test across experiments on the average lateral deviation before the crossing of the threshold position of baseline trials following curl field trails, it was proven that the after-effect was larger in the low frequency experiment than in the high frequency experiment, as illustrated in figure 5.2. This decrease in after-effect linked to the increase of uncertainty of the context, suggests that the controller is less adapted in a less predictable context. The rate of adaptation k, as defined in equation 5.1, was quantified for both experiments.

#### Quantification of the rate of adaptation k

The rate of adaptation was quantified for both experiments by evaluating the ratio of the after-effect due to a curl force field trial to the lateral deviation of the hand path during that same curl force field trial. The results obtained were averaged across experiments and gathered in table 4.5, showing that on average, baseline trials of the low frequency experiment showed a 21.3% adaptation to the experienced curl force fields whereas trials of the high frequency experiment showed a 17.3% adaptation to the same experienced curl force fields. These results suggest that baseline trials of the low frequency experiment showed a 4% higher adaptation to curl force field trials than baseline trials of the high frequency experiment. Therefore, our experiment suggests that the rate of adaptation is predicted by the uncertainty of the environment. A higher rate of adaptation is used by the controller in a more predictable context.

### 5.2.2 Forward velocity

The modulation of the peak forward hand velocity across contexts was analysed in section 4.2.2. The mean peak forward hand velocity was plotted for baseline trials of index 0, 1 and 2 and for the low and high frequency experiment with a 95% confidence interval on figure 4.9. A clear increase in forward hand velocity is noticeable both for an increase in index and an increase in uncertainty of context. These results were also statistically confirmed by computing an ANOVA and a t-test. The increase in peak forward velocity

measured in the high frequency experiment coincides with the prediction of a more robust controller in a less predictable context.

As explained in section 2.2.2, the forward hand velocity is a variable that allows us to measure the changes in control gains. Therefore, our results suggest that on average, the control gains were higher in the high frequency experiment than in the low frequency experiment. Simultaneously, our results suggest that the control gains evolve within each context according to the experienced perturbations. For both experiments, higher peak forward velocities were measured during baseline trials of a higher index, indicating that the control gains are increased after each perturbation.

The relative variation in peak forward hand velocity of each participant in both contexts was also analysed in section 4.2.2. The peak forward hand velocities of each subject were averaged across trial indexes in both experiments, i.e. an average peak velocity was computed per subject and per context. This average was then subtracted from the previously computed peak forward velocities of each subject, index and context. The resulting outcome was plotted in figure 4.10.

The plots of figure 4.10 illustrate how the peak velocity, and thus the control gains, evolved as a function of the baseline index for each participant in both contexts, independent of any differences in sample means. The relative increase in peak forward velocity seemed less variable from participant to participant in the high frequency experiment than in the low frequency experiment. To confirm this hypothesis, a levene test was computed. The levene test was used to determine whether the variance of the relative peak forward hand velocity curves was the same in both experiments. A p-value of 0.0918 was calculated. It could therefore not be statistically proven that a difference in distribution exists between both experiments.

However, even though the p-value obtained was bigger than the chosen threshold of 0.05, it remains quite small ($< 0.1$). Therefore, it could be that the results were not significant enough due to the small sample size used, but that a true difference in variance exists between both experiment. This change in variance would mean that the control gains are not only smaller in the low frequency experiment, but that they are also more variable. In other words, an increase of environment uncertainty would lead to larger and "more controlled" control gains, which have a higher baseline level and are regulated according to the experienced disturbances in an well-organized and controlled way. It is our hypothesis that the controller attributes greater focus on the modulation of the control gains in a less certain environment, generating smaller variances in the relative changes of control gains according to baseline index. However, this hypothesis could not be confirmed due to the small sample size used. Verifying this hypothesis constitutes work for further research.

### 5.2.3 Robustness

The between context analysis of the robustness to perturbations was analysed for curl force field trials. As illustrated by figure 4.14, the lateral deviation of the hand trajectory of responses to curl field trials was bigger for trials of the low frequency experiment than trials of the high frequency experiment. This was also statistically proven in section 4.3.2, by comparing the maximum lateral deviations of curl force field trials of both experiments.

These results suggests once again that the control gains of the controller were higher in the high frequency experiment than in the low frequency experiment. Indeed, as explained in section 2.2.2, an increase in control gains leads to more robust responses to perturbations.

### 5.2.4 Co-contraction

The between context analysis of co-contraction was performed both for baseline trials and curl force field trials. The results showed, in figure 4.17 and 4.18, that in both cases the trials of the high frequency experiment presented higher muscle activity than the trials of the low frequency experiment. These results were also statistically proven in section 4.4.2. Therefore, our predictions presented in section 2.2.2, suggesting that co-contraction is used to alter the control gains, were confirmed. Indeed, the increase in co-contraction between the low and high frequency experiment, correlated with the increase in forward velocity and robustness to responses, which are variables that indicate the increase in control gains.

### 5.2.5 Trade-off between adaptive and robust control

Altogether, the changes across experiments in after-effect, forward velocity, robustness to perturbations and co-contraction of the pectoralis major and posterior deltoid showed evidence of a change of control strategy and a change of adaptation linked to the change of environment uncertainty. Higher control gains where noticed in a less predictable environment, suggesting an increase of controller robustness linked to an increase of environment uncertainty. Simultaneously, the rate of adaptation used by the controller was noticed to decrease as the environment got less certain.

Therefore, it seems that to some extent, a trade-off exists between adaptive and robust control. Both strategies were noticed to be used simultaneously, but the increase of the use of one strategy seems to generate the decrease of the use of the second strategy. Based on these observations and the existing literature [8][6], a scientific question emerges on the nature of this trade-off between both strategies. To try and answer this question, the neural structures involved in modulating both strategies were analysed.

Studies have shown that patients with upper motor neuron lesions, who develop muscle over-activity called spasticity, exhibit abnormal co-contraction of agonist and antagonist muscle pairs [25]. This suggests that the antagonist inhibition, or reduction of activity, is mediated by the primary motor cortex [9]. Thus, it is possible that the "amount" of robustness used by the controller is, at least partially, modulated by the primary motor cortex, as it is responsible for the inhibition of antagonist muscle groups. On the other hand, adaptive control depends on higher level structures, including the cerebellum and the cortex. The cortex is used as sensorimotor interface and the cerebellum plays an important role in updating the internal representation of the movement dynamics [2][15]. Indeed, studies have shown that cerebellar damage can profoundly inhibit learning, due to dysfunctional updating of the internal models [26].

One should recall that the robust control was expressed in the context where higher levels of co-contraction were observed. Thus, assuming that the role of the cortex is to reduce co-contraction, it is conceivable that the default strategy used by the CNS is robust control,

and that it is the job of the cortex to reduce co-contraction to modulate the robustness of the controller. However, the question remains as to why the robustness of the controller seems to interfere with its ability to adapt to unexpected disturbances. Two possible hypotheses were suggested to answer this question.

Our first guess is that the higher level structures involved in adaptation, the cortex and the cerebellum, receive less sensory information due to the robustness of the controller, and therefore cannot adapt as much to the experienced perturbation. Indeed, the impact of a perturbation is smaller when working with a more robust controller, leading to smaller hand path errors. Additionally, studies have suggested that the degree of hand path error of the previous movement is correlated with the adaptation rate of the current movement [1]. Thus, a more robust controller leads to smaller hand path errors which lead to less adaptation. This hypothesis suggests that the trade-off between adaptive and robust control is based on a biological constraint.

An alternative guess is that the trade-off is not a consequence of a biological constraint, but rather the solution of an optimisation problem. We know that adaptive control is less costly, as robust control involves the increase in activity of both muscles. However, it is only efficient in a predictable context as it is only useful to update the internal representation of the movement dynamics according to an experienced perturbation, if these changes are likely to remain. In a very unpredictable context, the movement dynamics are constantly changed, and it is therefore not efficient to adapt the internal representation of the controller after each experienced perturbation. Hence, robust control is preferred in a less predictable context, as it does not need to know these changes in movement dynamics to handle the unexpected disturbances. This second hypothesis suggests that for a given environment uncertainty, the controller solves an optimisation problem to determine the optimal dosage of robustness and adaptation to use, such that the unexpected dynamics are correctly handled, while minimising the costs.

To conclude, based on our results a trade-off was noticed between adaptive and robust control in human reaching movements. The fundamental nature of this trade-off remains unknown. However, we presented two different hypotheses on the nature of this trade-off, the first one was based on a biological constraint of the neural structures involved in both strategies and the second one was based on the choice of an optimal strategy via the solving an optimization problem. Figuring out the true nature of this trade-off is an important challenge for future work, which will be discussed in section 5.5.

## 5.3 Choice of contexts

The goal of this master thesis was to analyse the modulation of the CNS's control strategy across contexts. More specifically the control strategy used by the CNS when executing reaching movements was studied in two different experiments, the low frequency experiment and the high frequency experiment, in which the uncertainty of the environment was modified. The task instructions were the same for both experiments, as explained in section 3.2. The two experiments only differed in the number and types of perturbations applied randomly during the reaching movements of a block of 60 trials. The environment variability and consistency were thus simultaneously modified, leading to a global change in uncertainty. Indeed, because both experiments did not contain the same number and

same types of perturbed trials, the probability of a certain trial occurring was not the same in both experiments. It is this change in probability that led to a difference in environment uncertainty between both experiments. The high frequency experiment consisted in a less predictable environment compared to the low frequency experiment.

This can be proven by computing the entropy of a block of trials in both experiments. The entropy is the mean information linked to the instances of a variable [17]. It can be interpreted as the uncertainty of the output of an event. In this case the instances are the different types of trials that can occur, and the entropy represents the uncertainty of picking one trial at random out of the set of 60 trials of the experiment block. The different instances, in this case trials, can be defined as follows:

- $x_1$ : baseline trial.
- $x_2$ : counter-clockwise curl force field trial.
- $x_3$ : clockwise curl force field trial.
- $x_4$ : leftward orthogonal force field trial.
- $x_5$ : rightward orthogonal force field trial.
- $x_6$ : leftward step-load trial.
- $x_7$ : rightward step-load trial. .

The formula used to compute the entropy is the following:

$$H(X(n)) = -\sum_{k=1}^{D} p_k \log_2 p_k \tag{5.2}$$

where $p_k = P(X(n)) = x_k)$ and $D$ is the size of the set of instances, which in this case is equal to 7.

| | $\mathbf{p}_{k,\ \textit{Low freq.}}$ | $\mathbf{p}_{k,\ \textit{High freq.}}$ |
|---|---|---|
| $\mathbf{x_1}$ | $\frac{50}{60}$ | $\frac{30}{60}$ |
| $\mathbf{x_2}$ | $\frac{5}{60}$ | $\frac{5}{60}$ |
| $\mathbf{x_3}$ | $\frac{5}{60}$ | $\frac{5}{60}$ |
| $\mathbf{x_4}$ | 0 | $\frac{5}{60}$ |
| $\mathbf{x_5}$ | 0 | $\frac{5}{60}$ |
| $\mathbf{x_6}$ | 0 | $\frac{5}{60}$ |
| $\mathbf{x_7}$ | 0 | $\frac{5}{60}$ |

**Table 5.1:** Probability distribution of the trial type in both experiments.

Using the probability distribution of the different instances of the trial type of both experiments, which is summarized in table 5.1, the entropy can be computed for both

experiments:

$$H_{Low} = -\frac{50}{60}\log_2\frac{50}{60} - 2 * \frac{5}{60}\log_2\frac{5}{60} = 0.817$$
$$H_{High} = -\frac{30}{60}\log_2\frac{30}{60} - 6 * \frac{5}{60}\log_2\frac{5}{60} = 2.292$$

The entropy of the low frequency experiment is lower than the entropy of the high frequency experiment. The context of the low frequency experiment is thus more certain than the context of the high frequency experiment. Therefore, using both contexts for a same reaching task allows us to analyse the controller's change of strategy across changes of predictability, which was the goal of this experiment.

### Contexts' influence on adaptive and robust control

The results obtained suggested an increase in rate of adaptation linked to a decrease of environment uncertainty and an increase in robustness linked to an increase of environment uncertainty. These results match discoveries that have already been stated in the literature, more specifically in an article published in 2014 that studied the rate of motor adaptation [6]. In this article the rate of motor adaptation and the feedback response strength were analysed as a function of both the variability and the consistency of the environment, which are two parameters that influence the global uncertainty of the environment. It was shown that the next-trial rate of motor adaptation is predicted by the environment consistency and not by its variability, but that the same-trial feedback response strength is determined by environmental variability rather than environmental consistency.

In our experiment, we did not dissociate the impact of environment consistency and environment variability on the rate of motor adaptation and the feedback response strength. It is the total uncertainty, based on both the consistency and the variability of the environment, which was modified across contexts. The increase of environment uncertainty of the context was obtained by increasing the number of perturbations and the different types of perturbations. Thus, it was obtained by increasing the environment variability and decreasing the environment consistency. Our results measured lower levels of adaptation in a less consistent environment and higher control gains in a more variable environment, which coincides with the results of the 2014 paper on the rate of motor adaptation [6].

However, it is impossible to determine whether the changes in motor adaptation and robustness were indeed respectively due to the changes of environment consistency and environment variability, as both parameters were modified simultaneously in our experiment. We have thus evaluated the changes in control strategy across changes in global environment uncertainty, but evaluating these changes across changes in environment consistency and environment variability separately constitutes work for further research.

## 5.4 Complications and constraints

### Dataset size

A major drawback of the experiment conducted was the sample size used. A group of 7 participants took part in our experiment, instead of the originally planned sample size of 18. This limitation in number of participants was due the Covid-19 crisis. Thankfully, we were still able to obtain statistically significant results despite the low sample size. Based on the effect size of the variables compared, we were able to declare that the results were significant [10]. However, expanding the sample size would enable us to obtain more precise results.

### Linear model of the arm

The control theories developed in this paper are based on the control designs presented in the 2019 paper on robust control. The robust control design used forced us to consider a linear state-space representation of the arm. Because the true dynamics of the arm aren't linear, the model used doesn't capture the true dynamics. A more precise control design could be used by linearising the system around a state or trajectory across time and space and computing the optimal control command locally [8].

## 5.5 Further perspectives

In this section we discuss different ideas on how to improve the work done in this master thesis.

### Modulation of control strategies across changes of environment variability and environment consistency

The modulation of the control strategy used by the CNS was analysed across a change of environment uncertainty. Studies have shown that the adaptation rate is predicted by environment consistency whereas the feedback response strength is predicted by environment variability, as explained in section 5.3. Thus, analysing the changes in after-effect, forward velocity, robustness of responses to perturbations and co-contraction of the PM and PD when only one of both parameters (variability or consistency) of the environment is modified, would allow us to confirm these results and acquire better knowledge of the changes in control strategy and adaptation across changes of context.

### Relative forward hand velocity analysis

In section 4.2.2, the relative increase in peak forward hand velocity according to baseline index was compared across both experiments. A difference in variance was noticed in figure 4.10, however this difference could not be proved to be statistically significant due to the small sample size used. Therefore, expanding the sample size used to determine whether a statistically significant difference in variance between both experiments exists, is an important analysis for further research.

**Trade-off between adaptive and robust control.**

Based on our results a trade-off was shown to exist between adaptive and robust control in human reaching movements, as explained in section 5.2.5. Two different hypotheses as to why this trade-off exists were presented. The first one was based on a biological constraint of the neural structures involved in both strategies and the second one was based on the choice of a strategy via the solving an optimization problem. However, the true scientific nature of this trade-off remains unknown. Further research is required to confirm or reject these hypotheses. For instance, the cost and efficiency of each strategy could be evaluated numerically according to the environment uncertainty, to see whether an optimization problem exists resulting in the same "amount" of robustness and adaptation for each environment uncertainty.

# Chapter 6

# Conclusion

In this master's thesis we have achieved our main goal, which was to analyse the modulation of the control strategy used by the CNS across contexts. We have discovered that a more robust strategy is used in a less predictable context, which was noticed to occur at the expense of adaptation.

Going back to our illustrative example of section 1.1, we now know how a professional wrestler would modulate his control strategy across contexts. When in the fighting ring, which stands for a very unpredictable environment, the CNS of the wrestler will likely increase the robustness of the controller to counter the very unpredictable disturbances. Simultaneously, the rate of adaptation used by the controller will be diminished. On the other hand when in the supermarket, which stands for a very predictable environment in which unexpected perturbations are unlikely, the CNS of the wrestler will decrease the robustness of the controller and increase its rate of adaptation.

Furthermore, we developed different hypotheses as to why these changes of strategy and adaptation occur. We believe that it is either a biological constraint of the neural structures, or the resolution of an optimization problem on the amount of robustness and adaptation that should be used by the controller, that prevents both strategies from being used to their fullest simultaneously. However, these hypotheses have yet to be proven.

# Bibliography


[1] Scott T Albert and Reza Shadmehr. "The neural feedback response to error as a teaching signal for the motor learning system". In: *Journal of Neuroscience* 36.17 (2016), pp. 4832–4845.

[2] John S Barlow. *The cerebellum and adaptive control*. Cambridge University Press, 2005.

[3] Tamer Başar and Pierre Bernhard. "A General Introduction to Minimax (H∞-Optimal) Designs". In: *H∞-Optimal Control and Related Minimax Design Problems*. Springer, 2008, pp. 1–32.

[4] Etienne Burdet et al. "A method for measuring endpoint stiffness during multi-joint arm movements". In: *Journal of biomechanics* 33.12 (2000), pp. 1705–1709.

[5] Etienne Burdet et al. "The central nervous system stabilizes unstable dynamics by learning optimal impedance". In: *Nature* 414.6862 (2001), pp. 446–449.

[6] Luis Nicolas Gonzalez Castro et al. "Environmental consistency determines the rate of motor adaptation". In: *Current Biology* 24.10 (2014), pp. 1050–1061.

[7] Frédéric Crevecoeur and Stephen H Scott. "Beyond muscles stiffness: importance of state-estimation to account for very fast motor corrections". In: *PLoS computational biology* 10.10 (2014).

[8] Frédéric Crevecoeur, Stephen H Scott, and Tyler Cluff. "Robust control in human reaching movements: a model-free strategy to compensate for unpredictable disturbances". In: *Journal of Neuroscience* 39.41 (2019), pp. 8135–8148.

[9] Bernard Dan et al. "Adaptive motor strategy for squatting in spastic diplegia". In: *European journal of paediatric neurology* 3.4 (1999), pp. 159–165.

[10] Joost CF De Winter. "Using the Student's t-test with extremely small sample sizes". In: *Practical Assessment, Research, and Evaluation* 18.1 (2013), p. 10.

[11] Wilhelm Flügge. *Viscoelasticity*. Springer Science & Business Media, 2013.

[12] David W Franklin et al. "Adaptation to stable and unstable dynamics achieved by combined impedance control and inverse dynamics model". In: *Journal of neurophysiology* 90.5 (2003), pp. 3270–3282.

[13] Yuan-cheng Fung. *Biomechanics: mechanical properties of living tissues*. Springer Science & Business Media, 2013.

[14] Donald E Kirk. *Optimal control theory: an introduction*. Courier Corporation, 2004.

[15] Mark Laubach, Marcelo S Caetano, and Nandakumar S Narayanan. "Mistakes were made: neural mechanisms for the adaptive control of action initiation by the medial prefrontal cortex". In: *Journal of Physiology-Paris* 109.1-3 (2015), pp. 104–117.

[16] C Elaine Little et al. “Test–retest reliability of KINARM robot sensorimotor and cognitive assessment: in pediatric ice hockey players”. In: *Journal of neuroengineering and rehabilitation* 12.1 (2015), p. 78.

[17] Benoit Macq. *Information theory and coding Part I : Source Coding Engineering*. 2015.

[18] Healthline’s Medical Network. *Human Body > Muscular System > Muscles*. 2015. URL: `https://www.healthline.com/human-body-maps/shoulder-muscles#1`.

[19] Daniele Piscitelli. “Motor rehabilitation should be based on knowledge of motor control”. In: *Archives of physiotherapy* 6.1 (2016), p. 5.

[20] J Andrew Pruszynski et al. “Temporal evolution of "automatic gain-scaling"”. In: *Journal of neurophysiology* 102.2 (2009), pp. 992–1003.

[21] Jerome N Sanes, Bozhidar Dimitrov, and Mark Hallett. “Motor learning in patients with cerebellar dysfunction”. In: *Brain* 113.1 (1990), pp. 103–120.

[22] Brian B Schultz. “Levene’s test for relative variation”. In: *Systematic Zoology* 34.4 (1985), pp. 449–456.

[23] Stephen H Scott. “Optimal feedback control and the neural basis of volitional motor control”. In: *Nature Reviews Neuroscience* 5.7 (2004), pp. 532–545.

[24] Reza Shadmehr and Ferdinando A Mussa-Ivaldi. “Adaptive representation of dynamics during learning of a motor task”. In: *Journal of neuroscience* 14.5 (1994), pp. 3208–3224.

[25] G Sheean. “The pathophysiology of spasticity”. In: *European journal of neurology* 9 (2002), pp. 3–9.

[26] Maurice A Smith and Reza Shadmehr. “Intact ability to learn internal models of arm dynamics in Huntington’s disease but not cerebellar degeneration”. In: *Journal of neurophysiology* 93.5 (2005), pp. 2809–2821.

[27] Yuki Ueyama. “Mini-max feedback control as a computational theory of sensorimotor control in the presence of structural uncertainty”. In: *Frontiers in computational neuroscience* 8 (2014), p. 119.

[28] Dennis Wackerly, William Mendenhall, and Richard L Scheaffer. *Mathematical statistics with applications*. Cengage Learning, 2014.

**UNIVERSITÉ CATHOLIQUE DE LOUVAIN**
**École polytechnique de Louvain**
Rue Archimède, 1 bte L6.11.01, 1348 Louvain-la-Neuve, Belgique | **www.uclouvain.be/epl**